Received: Added at production | Revised: Added at production | Accepted: Added at production

DOI: xxx/xxxx

ARTICLE TYPE

Pseudospectral method for assessing stability robustness for linear time-periodic delayed dynamical systems

Francesco Borgioli[1] | David Hajdu[2,3] | Tamas Insperger[2,4] | Gabor Stepan[2,5] | Wim Michiels[1]

[1]Department of Computer Science, KU Leuven, Belgium
[2]Department of Applied Mechanics, Budapest University of Technology and Economics, Hungary
[3]MTA-BME Lendület Machine Tool Vibration Research Group, Budapest, Hungary
[4]MTA-BME Lendület Human Balancing Research Group, Budapest, Hungary
[5]MTA-BME Research Group on Dynamics of Machines and Vehicles, Budapest, Hungary

Correspondence
Francesco Borgioli, Department of Computer Science, KU Leuven, Celestijnenlaan 200A, Leuven 3001, Belgium. Email: francesco.borgioli@cs.kuleuven.be

Summary

The paper presents a pseudospectral approach to assess the stability robustness of linear time-periodic delay systems, where periodic functions potentially present discontinuities and the delays may also periodically vary in time. The considered systems are subject to linear real-valued time-periodic uncertainties affecting the coefficient matrices, and the presented method is able to fully exploit structure and potential interdependencies among the uncertainties. The assessment of robustness relies on the computation of the *pseudospectral radius* of the monodromy operator, namely the largest Floquet multiplier that the system can attain within a given range of perturbations. Instrumental to the adopted novel approach, a solver for the computation of Floquet multipliers is introduced, which results into the solution of a generalized eigenvalue problem which is linear w.r.t. (samples of) the original system matrices. We provide numerical simulations for popular applications modeled by time-periodic delay systems, such as the inverted pendulum subject to an act-and-wait controller, a single-degree-of-freedom milling model and a turning operation with spindle speed variation.

KEYWORDS:
Optimization, Differential equations, Spectral, Vibrations, Stability, Dynamical systems

1 | INTRODUCTION

With the requirement of the increasing precision of mathematical descriptions, many engineering applications are modeled by differential equations involving delays and periodic terms. Examples of applications modeled by time-periodic systems with delays can be found in different fields, such as machine tools vibrations[1,2], robotic systems[3], neural networks[4] and optimal control[5]. In this paper, we address the stability and robust stability of systems of time-periodic delay differential equations (TPDDEs) defined as follows

$$\dot{x}(t) = \sum_{i=1}^{m} A_i(t)x(t-\tau_i), \qquad t \geq 0, \tag{1}$$

where $x(t) \in \mathbb{C}^n$ for each t, the delay values are nonnegative real numbers and functions A_i satisfy $A_i \in \mathcal{R}(T)^{n\times n}$, where $\mathcal{R}(T)$ is the set of continuous real-valued periodic functions with main period equal to $T > 0$ which we formally define as follows

$$\mathcal{R}(T) = \{f : \mathbb{R} \mapsto \mathbb{R} | f(t) = f(t+T)\ \forall\, t \in \mathbb{R}\ , f \text{ is continuous}\}.$$

Extensions to piecewise-continuous coefficient matrices and periodically varying delays are briefly discussed in Section 4 and Section 5.

For time-invariant linear delay systems, the stability can be assessed by the real parts of the roots of the associated characteristic equation: we refer the interested reader to some popular monographs in the field[6,7]. On the other hand, the stability of delay-free time-periodic systems[8], respectively TPDDEs[9,10], is determined by the modulus of the eigenvalues of a linear operator with finite dimension, respectively infinite dimension, which is the so-called *monodromy operator*.

In the following, we briefly summarize the basic notions of the Floquet theory for TPDDE (1), assuming that $0 \leq \tau_1 < \cdots < \tau_m =: \tau_{\max}$; for a more detailed introduction, we refer the reader to some monographs[9,10,11]. Let $X = C([-\tau_{\max}, 0],\ \mathbb{R}^n)$ be the space of continuous functions from interval $I = [-\tau_{\max}, 0]$ to $\mathbb{R}^n$; we now introduce the Cauchy problem

$$\begin{cases} \dot{x}(t) = \sum_{i=1}^{m} A_i(t)x(t-\tau_i), & t \geq t_0, \\ x(t_0+t) = \varphi(t), & t \in [-\tau_{\max}, 0], \end{cases} \tag{2}$$

with $\varphi \in X$: the problem admits a unique solution in the interval $[t_0 - \tau_{\max}, +\infty)$. In the following, we will indicate this solution as $x(t; t_0, \varphi)$ for $t \geq t_0$. The corresponding *state* at time t is denoted by $x_t(t_0, \varphi) \in X$, formally defined by

$$x_t := x(t+\theta), \qquad \theta \in [-\tau_{\max}, 0]. \tag{3}$$

Given the well-posedness of the Cauchy problem, we can introduce the notion of *evolution operator*.

Definition 1. The evolution operator is the operator $\mathcal{T}(t, t_0) : X \mapsto X$ associating the initial function $\varphi \in X$ with the state x_t at the time $t \geq t_0$, i.e.,

$$\mathcal{T}(t, t_0)\varphi = x_t(t_0, \varphi).$$

This definition is suitable for any system of non-autonomous differential equations, thus the periodicity is not required. When we consider time-periodic systems, then we rather use the *monodromy operator* $U := \mathcal{T}(T, 0)$, where T is the main period of our system of interest. It can be proved that the spectrum $\sigma(U)$ of the monodromy operator U is an at most countable compact set of $\mathbb{C}$ with the only possible accumulation point being zero. Moreover, it can be proved that if $\mu \in \sigma(U)$, then μ belongs to the spectrum of the evolution operator $\mathcal{T}(t_0 + T, t_0)$ for all $t_0 \in \mathbb{R}$. Therefore, the spectrum of the evolution operator $\mathcal{T}(t_0 + T, t_0)$ is independent of the choice of t_0.

Definition 2. Any element $\mu \in \sigma(U) \setminus \{0\}$ is called a Floquet multiplier.

Since all nonzero elements of the spectum of U correspond to eigenvalues, a Floquet multiplier can alternatively be defined as $\mu \in \mathbb{C},\ \mu \neq 0$, such that $\ker(\mu I - U) \neq \{0\}$. A graphical interpretation of the action of the monodromy operator U is provided in Figure 1. The following two propositions characterize the importance of Floquet multipliers in the stability investigation of TPDDEs.

Proposition 1. An element $\mu \in \mathbb{C},\ \mu \neq 0$, is a Floquet multiplier if and only if there exists an eigenfunction $\varphi \in X,\ \varphi \neq 0$, such that $\mathcal{T}(t + T, 0)\varphi = \mu\mathcal{T}(t, 0)\varphi$ for all $t \geq 0$.

Proposition 2. The zero solution of (2) is uniformly asymptotically stable if and only if all the Floquet multipliers of the associated monodromy operator have modulus smaller than 1.

In the literature, the stability analysis of many engineering applications modelled with TPDDEs rely on Floquet theory and on the computation of the Floquet multipliers, for which many methods are already available: examples are the semi-discretization method[12,13], the Galerkin based spectral element method[14,15], the pseudospectral collocation method[11,16] or the truncation of the monodromy operator expanded in Chebyshev series[17]. However, as uncertainties are always present in the models, a numerically predicted system stability does not always correspond to the system stability in practice. As a matter of fact, the presence of uncertainties affecting our system necessarily alters the Floquet multipliers, and potentially leads to instability. In this work we address the stability robustness problem by investigating the worst-case setting for a given class of uncertainties perturbing the nominal matrices, i.e., for the first time we extend the concept of pseudospectrum from autonomous to time-periodic systems: in practice, once established the class of perturbations to which our system is subjected and the maximum magnitude allowed, we look for the largest (in magnitude) Floquet multiplier that can be generated by any perturbation contained in the examined class, which we defined as the *Floquet pseudospectral radius*. The solution of our system will then be asymptotically stable (despite the uncertainties) if and only if the Floquet pseudospectral radius has modulus less than one.

To the best of the authors' knowledge, this is the first eigenvalue-based approach to the stability robustness of TPDDEs with uncertainties in the coefficient matrices; moreover, the method proposed here exploits a necessary and sufficient condition for the stability robustness. A Lyapunov-Krasovskii approach to the problem was previously proposed[18]. Similar problems to the one here addressed were considered in the literature, mainly regarding discrete-time problems: for example, stability criteria[19]

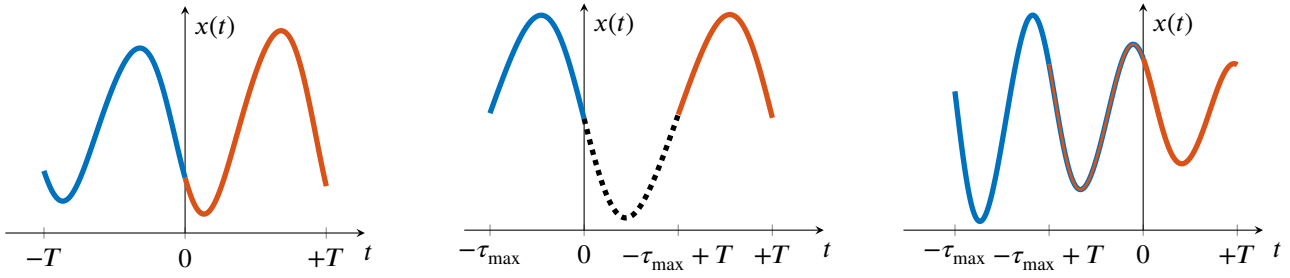

(a) $T = \tau_{\max}$ **(b)** $T > \tau_{\max}$ **(c)** $T < \tau_{\max}$

FIGURE 1 The plots show the action of monodromy operator U relating state x_0 in blue with state x_T in red for three different cases: in 1a $T = \tau_{\max}$, in 1b $T > \tau_{\max}$ and finally in 1c $T < \tau_{\max}$ (notice that in this latter case the two states overlap). In particular we here observe the effect of U on eigenstate x_0 such that $x_T = Ux_0 = \mu x_0$, with Floquet multiplier μ such that $|\mu| > 1$ (1a), $|\mu| = 1$ (1b) and $|\mu| < 1$ (1c).

independent of the time-delay length were proposed for discrete TPDDEs, and a robust stabilization technique for such problems was also suggested[20].

Instrumental to analysis of the stability robustness, we first introduce a solver for the computation of Floquet multipliers. The solver is based on a spectral discretization of the solution operator, which is accomplished with a collocation approach resulting in the approximation of the eigenfunctions of (2) with piecewise polynomials. The proposed solver results in the solution of a generalized eigenvalue problem (GEP) whose dimensions depend on the degree of the piecewise polynomial. The main benefit of the solver is that it preserves linearity w.r.t. entries of nominal matrices A_i. As a consequence, *linear real-valued structured* perturbations on matrices A_i result in *linear real-valued structured* perturbations of the formulated GEP, where with the term *structured* we mean that any specific structure can be considered for the uncertainty (thus a block or a single coefficient of the nominal matrix can be perturbed). As will be made clear in Section 3, this enables us to use an explicit expression for the derivative of an (approximated) Floquet multiplier w.r.t. some system parameters.

The computation of the Floquet pseudospectral radius is grounded in geometric optimization, i.e., it employs projected gradient techniques over manifolds[21] of matrices defined by the allowed perturbations. For the first time, this work extends to TPDDEs a state-of-the-art technique for the maximization of the spectral abscissa of eigenvalue problems[22,23], with the main difference being the objective function to be maximized (we here maximize the modulus of an eigenvalue, while this technique was commonly used to maximize the real part).

The paper is structured as follows: in Section 2, a generic description of a solver for computing Floquet multipliers based on a collocation approach is given; the description is generic in the sense that it applies for any choice of the discretization of the domain $[-\tau_{\max}, T]$, of the grid points and of the polynomial basis. The details of our implementation (which is made publicly available[24]), are reported in the Appendix, together with an explicit construction of the GEP for the special case where $T > \tau_{\max}$. In Section 3, we formally introduce the uncertainties affecting the system and we illustrate the algorithm implemented to assess the stability robustness. In Section 4, we apply our algorithm to well-known applications modelled by TPDDEs with piecewise-continuous periodic functions and constant delays: indeed, we analyse the stability robustness of linear systems with act-and-wait controllers (used for instance in applications such as the inverted pendulum for balancing problems[25,26]), and for a milling model with one degree of freedom. In Section 5 we then consider periodic systems with periodic delays, like the model of a turning operation with spindle speed variation, and we again perform an analysis of the stability robustness. Finally, in Section 6, we give our conclusions.

2 | A COLLOCATION-BASED SOLVER FOR FLOQUET MULTIPLIERS

In this section we present a high-level description of a solver to compute the Floquet multipliers of (1). Solutions of (2), corresponding to an eigenfunction of the monodromy operator, are approximated using piecewise polynomials, obtained by imposing collocation conditions. Few assumptions on the piecewise polynomial, the polynomial bases, and the meshes are taken in this

section. In this way, existing collocation-based schemes, such as the one in Chapter 6 of[11], the one implemented in DDE-BIFTOOL[16] or the routine to compute Floquet multipliers included in the COCO package[27] fit within the general scheme, while specific choices are also amendable for the extensions discussed in Sections 4-5. In the Appendix, we will provide the implementation details of our code which is made publicly available[24].

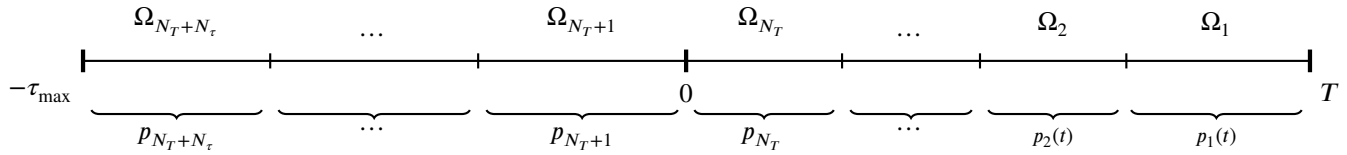

FIGURE 2 Generic discretization of the domain $[-\tau_{\max}, T]$ into N subintervals, for $N := N_T + N_\tau$.

Let us consider the interval $[-\tau_{\max}, T]$ and with no constraint on the ratio $T/\tau_{\max}$. As illustrated in Figure 2, we assume that interval $[-\tau_{\max}, 0]$, respectively $[0, T]$, is divided into N_τ, respectively N_T, subintervals Ω_j for $j = 1, \dots, N$ with $N := N_\tau + N_T$. We want to approximate the solution x of (1) with a piecewise polynomial p, so that an overall approximation of x can be formally defined as

$$x(t) \approx p(t) = \sum_{j=1}^{N} p_j(t)\chi_{\Omega_j}(t), \quad \text{for } t \in [-\tau_{\max}, T], \tag{4}$$

where χ_{Ω_j} is the indicator function of the subinterval Ω_j, defined as

$$\chi_{\Omega_j}(t) = \begin{cases} 1, \text{ if } t \in \Omega_j, \\ 0, \text{ elsewhere,} \end{cases}$$

and p_j is a polynomial. Let us set $M_j \in \mathbb{N}$ as the degree of each polynomial p_j, then its formal definition reads as follows

$$p_j(t) := \sum_{s=0}^{M_j} c_s^{(j)} T_s(t), \text{ for } j = 1, \dots, N, \ t \in [-\tau_{\max}, T], \tag{5}$$

where $\{T_s\}_{s=0}^{\infty}$ is a basis of polynomials, and $c_s^{(j)} \in \mathbb{C}^n$ are the associated coefficients to be determined: observe that in the case of a Lagrange basis, the coefficients $c_s^{(j)}$ would coincide with the values of p on a mesh over $[-\tau_{\max}, T]$.
Let us define $M_T := \sum_{j=1}^{N_T}(M_j + 1)$, $M_\tau := \sum_{j=1}^{N_\tau}(M_{j+N_T} + 1)$ and $M := M_T + M_\tau$. We then introduce the compact form $\vec{C} \in \mathbb{C}^{N_{\text{eqn}}}$, with $N_{\text{eqn}} := n \times M$, as the column vector containing all the coefficients $c_s^{(j)}$, which reads as

$$\vec{C} = [c_0^{(N)\top} \ \dots c_{M_N}^{(N)\top} \ \dots \ c_0^{(1)\top} \ \dots c_{M_1}^{(1)\top}]^\top. \tag{6}$$

It is instrumental to the definition of the interpolation operator $\mathcal{I}$,

$$\begin{aligned} \mathcal{I} : [-\tau_{\max}, T] \times \mathbb{N} &\mapsto \mathbb{R}^{n \times N_{\text{eqn}}} \\ (t, d) &\mapsto \mathcal{I}^{(d)}(t), \quad \text{such that} \quad \mathcal{I}^{(d)}(t)\vec{C} = p^{(d)}(t), \end{aligned} \tag{7}$$

which returns the value of the d-th derivative ($d \geq 0$) of the piecewise polynomial p at time t (at the end point of a subinterval one-sided derivatives are considered).

Now, we describe at a high level how solution x of (1), corresponding to an eigenfunction, is approximated by the piecewise polynomial p: from Proposition 1, we know that $\mu \neq 0$ is a Floquet multiplier if and only if there exists an eigenfunction φ such that

$$\mathcal{T}(t + T, 0)\varphi = \mu \mathcal{T}(t, 0)\varphi, \text{ for all } t \geq 0.$$

Then, setting $t = 0$, implies that

$$x_T(0, \varphi) = \mathcal{T}(T, 0)\varphi = \mu \mathcal{T}(0, 0)\varphi = \mu\varphi, \tag{8}$$

which is equivalent to

$$x(\theta + T; 0, \varphi) = \mu\varphi(\theta), \text{ for all } \theta \in [-\tau_{\max}, 0]. \tag{9}$$

Therefore, in order to calculate the Floquet multipliers we approximate the solutions x of equation (9), that is we approximate the solutions of the Cauchy problem (2) where the initial state φ is an (unknown) eigenfunction of the monodromy operator

U associated with (1). We then construct the piecewise polynomial p approximating x as follows. First, we require that it corresponds to a solution: this is done by imposing continuity at boundary points of subintervals Ω_j, and by imposing collocation requirements for the TPDDE (1) on $[0, T]$. Second, we require that the solution corresponds to an eigenfunction of U. This is done by imposing collocation conditions for the equation (9) on $[-\tau_{\max}, 0]$. The conditions defining such approximation give rise to the GEP

$$F(\mu)\vec{C} = (\mathcal{B} - \mu\mathcal{A})\vec{C} = 0, \tag{10}$$

with $\mathcal{A}, \mathcal{B} \in \mathbb{R}^{N_{\text{eqn}} \times N_{\text{eqn}}}$, and whose nonzero eigenvalues μ approximate the Floquet multipliers of the monodromy operator U associated with (1). At the end of this section we prove that solving the resulting GEP is equivalent to computing the eigenvalues of a matrix approximation of the monodromy operator.

In order to work out these conditions in detail, we now need to introduce meshes of our subdomains $[-\tau_{\max}, 0]$ and $[0, T]$. We consider two meshes $m_\tau := \{\theta_\tau^\ell\}_{\ell=1}^{\rho_\tau} \subset [-\tau_{\max}, 0]$ and $m_T := \{\theta_T^\ell\}_{\ell=1}^{\rho_T} \subset [0, T]$, such that $\rho_\tau = M_\tau$ and $\rho_T = M_T - N_T$. We only require that each subinterval Ω_j contains M_j points for $j = 1, \dots, N_T$ and $M_j + 1$ points for $j > N_T$, The reason for the choices of the number of points ρ_τ and ρ_T will be made clear in the following.

- For $j = 1, \dots, N_T$ we impose continuity of p in the left boundary point of the interval Ω_j (which we indicate with b_j), i.e., we require the following equation to be satisfied:

$$p_j(b_j) = p_{j+1}(b_j), \text{ for } j = 1, \dots, N_T.$$

- We impose the collocation constraints for TPDDE (1) on the mesh m_T, thus we set

$$\dot{p}(\theta_T^\ell) = \sum_{i=1}^{m} A_i(\theta_T^\ell) p\left(\theta_T^\ell - \tau_i\right), \quad \text{for each } \theta_T^\ell \in m_T,$$

  which is equivalent to

$$\left(\mathcal{I}^{(1)}(\theta_T^\ell) - \sum_{i=1}^{m} A_i(\theta_T^\ell)\mathcal{I}^{(0)}\left(\theta_T^\ell - \tau_i\right)\right)\vec{C} = 0, \quad \text{for each } \theta_T^\ell \in m_T. \tag{11}$$

  Notice that these conditions and the constraints of continuity in the boundary points b_j can be rewritten together into a compact matricial form as follows

$$M_1\vec{C} = 0, \tag{12}$$

  where $M_1 \in \mathbb{R}^{nM_T \times N_{eqn}}$.

- Expression (12) allows to compute an approximate forward solution provided that the initial function, in the form of the coefficients of $p_{N_T+1}, \dots p_{N_T+N_\tau}$ is given. We now express that this initial function approximates an eigenfunction, by imposing collocation constraints for (9). This leads us to

$$\mu p(\theta_\tau^\ell) = p(\theta_\tau^\ell + T), \text{ for each } \theta_\tau^\ell \in m_\tau,$$

  which is equivalent to

$$\mu\mathcal{I}^{(0)}(\theta_\tau^\ell)\vec{C} = \mathcal{I}^{(0)}(\theta_\tau^\ell + T)\vec{C}, \text{ for each } \theta_\tau^\ell \in m_\tau. \tag{13}$$

  With a little abuse of notation, this system of equations can be rewritten into a compact matricial form as

$$\mu \underbrace{\mathcal{I}^{(0)}(m_\tau)}_{:=B}\vec{C} = \underbrace{\mathcal{I}^{(0)}(m_\tau + T)}_{:=E}\vec{C}, \tag{14}$$

  where $B, E \in \mathbb{R}^{nM_\tau \times N_{eqn}}$, and the last nM_T columns of B contain only zeros. Observe then that the vector $B\vec{C}$, respectively $E\vec{C}$, contains the values of the piecewise polynomial p in the mesh points $\{\theta_\tau^\ell\}_{\ell=1}^{\rho_\tau} \subset [-\tau_{\max}, 0]$, respectively $\{\theta_\tau^\ell + T\}_{\ell=1}^{\rho_\tau} \subset [T - \tau_{\max}, T]$.

Now, our system in the coefficients $c_s^{(j)}$ has N_{eqn} equations, and thus it is square. Putting all the pieces together, equations (14) and (12) give rise to (10), with

$$\mathcal{A} = \begin{bmatrix} B \\ 0_{nM_T \times N_{eqn}} \end{bmatrix}, \quad \mathcal{B} = \begin{bmatrix} E \\ M_1 \end{bmatrix}.$$

In the above scheme, consistent with our implementation described in the Appendix, we only impose continuity for nonnegative t (in an explicit way[1]). Another option consists of reducing the number of collocation conditions for (9) with $N_\tau - 1$, and instead imposing continuity on the entire interval $[-\tau_{\max}, T]$. We note that in the case where the unknown coefficients represent function values on a mesh, and the submeshes are overlapping (common end points), continuity is already imposed by the parametrization, and only collocation requirements for (1) and (9) remain.

To conclude the section, we demonstrate that the Floquet multiplier approximations solving (10) could equivalently be obtained as eigenvalues of a properly defined finite dimensional approximation (i.e., a matrix approximation) of the monodromy operator U, which relates the discretized states function in the intervals $[-\tau_m, 0]$ and $[-\tau_m + T, T]$. Denote by x the vector of samples of an initial function for (1) at $t = 0$, obtained by evaluation on the mesh m_τ. Then an approximation of the emanating solution, in the form of piecewise polynomial (4), can be computed from

$$\begin{cases} M_1 \vec{C} = 0 \\ B\vec{C} = x \end{cases} \iff \vec{C} = \begin{bmatrix} M_1 \\ B \end{bmatrix}^{-1} \begin{bmatrix} 0 \\ x \end{bmatrix}.$$

Then, sampling the approximate solution in the points $\{\theta_\tau^\ell + T\}_{\ell=1}^{\rho_\tau} \subset [-\tau_m + T, T]$ gives

$$y = E\vec{C} = E \begin{bmatrix} M_1 \\ B \end{bmatrix}^{-1} \begin{bmatrix} 0 \\ x \end{bmatrix} = E \begin{bmatrix} M_1 \\ B \end{bmatrix}^{-1} \begin{bmatrix} 0 \\ I_{n\rho_\tau} \end{bmatrix} x := \widehat{U} x.$$

Therefore matrix $\widehat{U}$ is an approximation of monodromy operator U, and its eigenvalues $\mu \neq 0$ satisfy

$$\det\left(I_{n\rho_\tau} - \frac{1}{\mu} E \begin{bmatrix} M_1 \\ B \end{bmatrix}^{-1} \begin{bmatrix} 0 \\ I_{n\rho_\tau} \end{bmatrix} \right) = 0. \tag{15}$$

Some simple algebraic manipulations yields that (15) is equivalent to

$$\begin{cases} M_1 \vec{C} = 0, \\ E\vec{C} = \mu B \vec{C} \end{cases} \tag{16}$$

for some $\vec{C} \neq 0$, which on its turn corresponds to (10).

3 | WORST CASE ANALYSIS FOR FLOQUET MULTIPLIERS

In this section we make the leap from unperturbed systems of TPDDEs to perturbed systems affected by matrix uncertainties; we want to perform a worst-case analysis on the stability of system (1), namely we want to compute the largest modulus a Floquet multiplier can attain under a class of uncertainties with prescribed maximum magnitude. In the first subsection we formally introduce the space of uncertainties affecting system (1), and we show how matrix perturbations on system (1) are propagated on GEP (10); as we will see, linear uncertainties on matrices A_i result in linear perturbations of GEP (10). The worst-case analysis is then performed by adapting a strategy already used for time-invariant systems without[22] and with delay[23]; in the second and third subsections we present the algorithm, highlighting main differences and similarities.

3.1 | Matrix uncertainties: from the time-periodic system to the GEP

We consider a set of K independent real-valued matrix perturbations δA_k such that $\|\delta A_k\|_F \leq \varepsilon$, $\varepsilon > 0$, where with $\|M\|_F = \sqrt{\sum_{i,j} M_{i,j}^2}$ we refer to the Frobenius norm of a matrix; these uncertainties are included in our system (1) as follows

$$\dot{x}(t) = \sum_{i=1}^{m} \left(A_i(t) + \sum_{k=1}^{K} D_{i,k}(t) \delta A_k E_{i,k}(t) \right) x(t - \tau_i), \qquad t \geq 0, \tag{17}$$

where $D_{i,k}$, $E_{i,k}$ are time-dependent scaling matrices with time-periodic coefficients with period T. Their dimensions depend on the dimension of the associated uncertainty δA_k; then, for $\delta A_k \in \mathbb{R}^{p_k \times q_k}$, we have $D_{i,k} \in \mathcal{R}(T)^{n \times p_k}$, $E_{i,k} \in \mathcal{R}(T)^{q_k \times n}$. First, the introduction of $D_{i,k}$, $E_{i,k}$ allows us to define a (potentially) time-periodic uncertainty that affects only a submatrix of the

[1] if all intevals Ω_j, except for $\Omega_{N_T+N_\tau}$, have the same length and the degree M_j is independent of j, both variants are equivalent.

nominal A_i, i.e., a single parameter or a block. As a consequence, any structure can be defined for the perturbations affecting the nominal system. In the uncertainty description, more than one uncertainty δA_k can simultaneously affect the nominal matrix A_i; at the same time, uncertainty δA_k can affect more than one nominal matrix A_i. Note that if δA_k does not affect A_i, then we set $D_{i,k}(t) \equiv 0$ and $E_{i,k}(t) \equiv 0$ for each t. Second, by introducing weights in the auxiliary matrices $D_{i,k}(t)$, $E_{i,k}(t)$, it is possible to reduce a set of uncertainties with different magnitudes to a set of ε-bounded uncertainties for some $\varepsilon > 0$, i.e. such that

$$\|\delta A_k\|_F \leq \varepsilon,\ k = 1, \dots, K. \tag{18}$$

To illustrate the definition of auxiliary matrices $D_{i,k}(t)$ and $E_{i,k}(t)$, we provide an example based on a well-known system from the literature.

Example 1. We consider the delayed Mathieu equation of second order[12,28], which we recast in a system of first order ODEs as follows

$$\begin{bmatrix} 1 & 0 \\ 0 & 1 \end{bmatrix} \dot{x}(t) = \underbrace{\begin{bmatrix} 0 & 1 \\ -(\eta + \beta\cos(\omega t)) & 0 \end{bmatrix}}_{:=A_1(t)} x(t) + \underbrace{\begin{bmatrix} 0 & 0 \\ b_0 & 0 \end{bmatrix}}_{:=A_2(t)} x(t-\tau), \tag{19}$$

where ω is such that $T = 2\pi/\omega$ and the ratio τ/T is arbitrary. We here analyse five cases where the system is affected by different perturbations:

- Suppose we consider *unstructured perturbations* resulting in coefficient matrices $A_1(t) + \delta A_1$ and $A_2 + \delta A_2$ such that $\|\delta A_1\|_F \leq 0.1$ and $\|\delta A_2\|_F \leq 0.1$. Then we take $\varepsilon = 0.1$, $K = 2$ and set $D_{1,1} = E_{1,1} = D_{2,2} = E_{2,2} = I$, while $D_{1,2}(t) = D_{2,1}(t) = E_{1,2}(t) = E_{2,1}(t) = 0$.

- Suppose we want to impose two uncertainties on parameters η and b_0, such that $|\delta\eta| \leq 0.5$ and $|\delta b_0| \leq 0.1$. Then, we set $K = 2,\ \varepsilon = 1$, and
$$D_{1,1}(t) = \begin{bmatrix} 0 \\ 0.5 \end{bmatrix},\ E_{1,1}(t) = \begin{bmatrix} 1 \\ 0 \end{bmatrix}^\top,\ D_{2,2}(t) = \begin{bmatrix} 0 \\ 0.1 \end{bmatrix},\ E_{2,2}(t) = \begin{bmatrix} 1 \\ 0 \end{bmatrix}^\top,$$
while $D_{1,2}(t) = D_{2,1}(t) = [0\ 0]^\top$ and $E_{1,2}(t) = E_{2,1}(t) = [0\ 0]$.

- Suppose now that we want to impose two uncertainties $|\delta\beta| \leq 0.3$ and $|\delta b_0| \leq 0.1$. Then, we set $K = 2,\ \varepsilon = 1$, and
$$D_{1,1}(t) = \begin{bmatrix} 0 \\ 0.3 \end{bmatrix},\ E_{1,1}(t) = \begin{bmatrix} \cos(\omega t) \\ 0 \end{bmatrix}^\top,\ D_{2,2}(t) = \begin{bmatrix} 0 \\ 0.1 \end{bmatrix},\ E_{2,2}(t) = \begin{bmatrix} 1 \\ 0 \end{bmatrix}^\top,$$
while $D_{1,2}(t) = D_{2,1}(t) = [0\ 0]^\top$ and $E_{1,2}(t) = E_{2,1}(t) = [0\ 0]$.

- Suppose that we want to impose two uncertainties $|\delta\eta| \leq 0.5$ and $|\delta\beta| \leq 0.3$. Then, we set $K = 2,\ \varepsilon = 1$, and
$$D_{1,1}(t) = \begin{bmatrix} 0 \\ 0.5 \end{bmatrix},\ E_{1,1}(t) = \begin{bmatrix} 1 \\ 0 \end{bmatrix}^\top,\ D_{1,2}(t) = \begin{bmatrix} 0 \\ 0.3 \end{bmatrix},\ E_{1,2}(t) = \begin{bmatrix} \cos(\omega t) \\ 0 \end{bmatrix}^\top,$$
while $D_{2,1}(t) = D_{2,2}(t) = [0\ 0]^\top$ and $E_{2,1}(t) = E_{2,2}(t) = [0\ 0]$.

- Finally, suppose that parameters $\eta,\ \beta$ and b_0 are uncertain, and the perturbations are such that $\|[\delta\eta\ \delta\beta\ \delta b_0]^T\|_2 \leq 0.1$. Then we set $K = 1,\ \varepsilon = 1, \delta A_1 \in \mathbb{R}^{1\times 3}$, and
$$D_{1,1}(t) = \begin{bmatrix} 0 \\ 0.1 \end{bmatrix},\ E_{1,1}(t) = \begin{bmatrix} 1 & 0 \\ \cos(\omega t) & 0 \\ 0 & 0 \end{bmatrix},\ D_{2,1}(t) = \begin{bmatrix} 0 \\ 0.1 \end{bmatrix},\ E_{2,1}(t) = \begin{bmatrix} 0 & 0 \\ 0 & 0 \\ 1 & 0 \end{bmatrix}.$$

□

We now come back to (17). Indicating the set of uncertainties with $\Delta = \left(\delta A_1, \dots, \delta A_K\right) \in \mathbb{R}^* := \mathbb{R}^{p_1\times q_1} \times \cdots \times \mathbb{R}^{p_K\times q_K}$, we formally define a global measure of the uncertainty as follows

$$\|\Delta\| := \left\| \left[\|\delta A_1\|_F \ \dots\ \|\delta A_K\|_F \right]^\top \right\|_\infty. \tag{20}$$

It is easy to observe that considering an ε-bounded set of uncertainties Δ, i.e. assuming $\|\Delta\| \leq \varepsilon$, is equivalent to considering (18).

Now, adapting a definition from the worst-case analysis of linear autonomous systems, we define the ε-pseudospectrum of (17) as the union set of the Floquet multipliers originated by any ε-bounded perturbation of the matrices, and which formally reads

$$\mathcal{M}_\varepsilon := \bigcup_{\Delta \in \mathbb{R}^*, \|\Delta\| \leq \varepsilon} \left\{ \mu \in \mathbb{C} : \exists\, \Delta \text{ s.t. } \mu \text{ is a Floquet multiplier of (17)} \right\}. \tag{21}$$

The *pseudospectral radius* μ_ε of the monodromy operator U (or the Floquet *pseudospectral radius*) is then defined as

$$\mu_\varepsilon := \max\{|\mu| : \mu \in \mathcal{M}_\varepsilon\},$$

and it is the Floquet multiplier with maximum modulus in the ε-pseudospectrum $\mathcal{M}_\varepsilon$. Thanks to these definitions, it will be clearer why we defined our method as a "pseudospectral" approach to investigate the stability robustness: after the extension of the concept of pseudospectrum to periodic systems, we can then state that the solution of the uncertain system (17) is *robustly stable* if and only if the corresponding Floquet pseudospectral radius has modulus less than one. In the next subsection we investigate how uncertainties δA_k propagate on the GEP defined in (10) and resulting from the discretization of the monodromy operator..

3.1.1 | Defining the perturbed GEP

First of all, we observe that a potential uncertainty on matrices A_i only affects the collocation constraints for TPDDE (1), thus only matrix $\mathcal{B}$ of GEP (10). Now, given an uncertainty δA_k we want to define appropriate auxiliary matrices that propagate this uncertainty on GEP (10). Let us consider the nominal matrix $A_i(t)$ affected by a perturbation $D_{i,k}(t)\delta A_k E_{i,k}(t)$ for each $t \in [0, T]$. In our discretized version, we must consider the effect of this perturbation for each θ_T^ℓ with $\ell = 1, \dots, \rho_T$. Therefore, for each uncertainty δA_k, $k = 1, \dots, K$, affecting matrix A_i, $i = 1, \dots, m$, we define two matrices $\mathcal{D}_{i,k}^\ell \in \mathbb{R}^{N_{eqn} \times p_k}$, $\mathcal{E}_{i,k}^\ell \in \mathbb{R}^{q_k \times N_{eqn}}$ which propagate such uncertainty on GEP (10) for $t = \theta_T^\ell$, $\ell = 1, \dots, \rho_T$. Then an uncertainty δA_k is propagated on the GEP (10) by perturbing the matrix $\mathcal{B}$ with $\delta\mathcal{B}^{(k)} = -\sum_{i=1}^m \sum_{\ell=1}^{\rho_T} \mathcal{D}_{i,k}^\ell \delta A_k \mathcal{E}_{i,k}^\ell$, where the minus sign is inherited by equation (11).

Finally, the GEP associated with a system of TPDDEs perturbed by a set $\Delta = (\delta A_1, \dots, \delta A_K)$ corresponding to (17) reads as follows

$$F(\mu; \Delta)\vec{C} = \left[\left(\mathcal{B} - \sum_{k=1}^{K} \underbrace{\sum_{i=1}^{m} \sum_{\ell=1}^{\rho_T} \mathcal{D}_{i,k}^\ell \delta A_k \mathcal{E}_{i,k}^\ell}_{=-\delta\mathcal{B}^{(k)}} \right) - \mu\mathcal{A} \right] \vec{C} = \left[\left(\mathcal{B} + \sum_{k=1}^{K} \delta\mathcal{B}^{(k)} \right) - \mu\mathcal{A} \right] \vec{C} = 0. \tag{22}$$

In the Appendix we provide explicit expressions for the matrices $\mathcal{D}_{i,k}^\ell, \mathcal{E}_{i,k}^\ell$.

We have seen now that a set Δ of matrix uncertainties affecting a system of TPDDEs like in (17) defines a highly structured perturbation (22) of the GEP (10); thus the Floquet multipliers of the perturbed system (17) correspond to the nonzero eigenvalues of the perturbed GEP (22). We thus approximate the pseudospectrum $\mathcal{M}_\varepsilon$ defined in (21) with the structured pseudospectrum of the nominal GEP (10) defined as follows

$$M_\varepsilon := \bigcup_{\Delta \in \mathbb{R}^*, \|\Delta\| \leq \varepsilon} \left\{ \mu \in \mathbb{C} : \exists\, \Delta\,, \mu \neq 0 \text{ s.t. } \det F(\mu; \Delta) = 0 \right\}. \tag{23}$$

Therefore, we will approximate the pseudospectral radius of the monodromy operator U as the eigenvalue with largest modulus in M_ε. In the next subsection we illustrate the algorithm for the computation of this eigenvalue, which we call μ_ε.

3.2 | Algorithm to compute the Floquet *pseudospectral radius*

The worst-case analysis is executed by adapting gradient-ascent methods defined over matrix manifolds which are widely used in the pseudospectral approach to the worst-case analysis of time-invariant functional-differential equations, where the real part of rightmost point of the pseudospectrum (the so-called *pseudospectral abscissa*) must be computed; among others, these strategies were used to compute the pseudospectral abscissa of standard eigenvalue problems perturbed by either complex-valued[29] or real-valued[22] uncertainties. Analogous methods were used to compute the pseudospectral abscissa for nonlinear eigenvalue

problems with complex-valued uncertainties[30] and for delay eigenvalue problems with real-valued uncertainties[23]. A substantial difference between the cited references and the work here proposed is represented by the objective function maximized here, which is the modulus of an eigenvalue rather than its real part.

In this section we illustrate how the method to compute the pseudospectral abscissa of linear time-invariant delay systems[23] can be extended to our problem; for our case, we need to compute the largest (in modulus) eigenvalue of a GEP with highly structured real-valued perturbations. Although the underlying idea remains the same, besides the objective function also the eigenvalue problem here considered is different from the cited references: for these reasons we believe it is important to rewrite the method in a complete form. First of all, in the next lemma we report the well-known formula for the derivative of a simple eigenvalue of a general eigenvalue problem; we refer the reader interested in a proof to[31].

Lemma 1. Let $G : \mathbb{C} \to \mathbb{C}^{n\times n},\ \lambda \to G(\lambda,\theta)$ be an analytic function depending smoothly on a set of parameters $\theta \in \mathbb{R}^d$, and let $\hat{\mu}$ be a simple eigenvalue of eigenvalue problem $G(\lambda,\hat{\theta})y = 0$ such that $\hat{x}^* G(\hat{\mu},\hat{\theta}) = 0$ and $G(\hat{\mu},\hat{\theta})\hat{y} = 0$, with $\hat{x},\ \hat{y} \in \mathbb{C}^n$ with unit norm, and $\hat{x}^*$ the complex conjugate transpose of $\hat{x}$. Then there exists an open ball $\mathcal{D} \subset \mathbb{R}^d$, containing $\hat{\theta}$, and a differentiable function $\mu :\ \mathcal{D} \mapsto \mathbb{C}$ such that $\mu(\hat{\theta}) = \hat{\mu}$, we have $\det(G(\mu(\theta),\theta)) = 0$ for all $\theta \in \mathcal{D}$ and

$$\frac{\partial \mu}{\partial \theta_i}(\hat{\theta}) = -\frac{\hat{x}^* \dfrac{\partial G(\hat{\mu},\hat{\theta})}{\partial \theta_i}\hat{y}}{\hat{x}^* \dfrac{\partial G(\hat{\mu},\hat{\theta})}{\partial \lambda}\hat{y}}, \qquad i = 1,\dots,d. \tag{24}$$

Now, in order to find the so-called Floquet *pseudospectral radius*, i.e., the Floquet multiplier with largest modulus in the pseudospectrum (23), we must solve the following optimization problem

$$\begin{aligned} \max\ & |\mu|^2 \\ \text{s.t. }& F(\mu;\Delta)x = 0 \text{ for some } x \in \mathbb{C}^{N_{eqn}}, \\ & \Delta \in \mathbb{R}^*,\ \|\Delta\| \le \varepsilon. \end{aligned} \tag{25}$$

It is important to mention that the problem of maximizing the spectral radius generically leads to simple dominant Floquet multipliers. This is in contrast to the problem of minimizing spectral radii and spectral abscissae, where defective eigenvalues in the optima are common[29].

In the next theorem we characterize the set of optimal perturbations, namely the matrix perturbations generating the Floquet *pseudospectral radius*: in particular, we give an explicit formula for the optimal perturbations when the norm constraint is active.

Theorem 1. Let μ_ε be the Floquet multiplier with largest modulus in the ε-pseudospectrum (23). Assume it is a simple eigenvalue generated by some set of perturbations Δ. Let also x, y be respectively the left and the right eigenvectors of μ_ε (with unit norms) satisfying the condition

$$\xi := x^* \mathcal{A} y > 0, \tag{26}$$

and let

$$X = [\Re(x)\ \Im(x)], \quad Y = [\Re(y)\ \Im(y)], \quad \Gamma = \begin{bmatrix} \Re(\mu_\varepsilon) & \Im(\mu_\varepsilon) \\ -\Im(\mu_\varepsilon) & \Re(\mu_\varepsilon) \end{bmatrix},$$

where $\Re$, $\Im$ are the real and the imaginary parts, respectively.

For every $k \in \{1,\dots,K\}$, matrix $\sum_{i=1}^{m}\sum_{\ell=1}^{\rho_T} \mathcal{D}_{i,k}^{\ell^\top} X\Gamma Y^\top \mathcal{E}_{i,k}^{\ell^\top}$ is either zero or nonzero. In the latter case, the optimal perturbation δA_k satisfies

$$\delta A_k = -\varepsilon \frac{\sum_{i=1}^{m}\sum_{\ell=1}^{\rho_T} \mathcal{D}_{i,k}^{\ell^\top} X\Gamma Y^\top \mathcal{E}_{i,k}^{\ell^\top}}{\left\| \sum_{i=1}^{m}\sum_{\ell=1}^{\rho_T} \mathcal{D}_{i,k}^{\ell^\top} X\Gamma Y^\top \mathcal{E}_{i,k}^{\ell^\top} \right\|_F}. \tag{27}$$

Proof. Let us consider uncertainty δA_k, and let us indicate with $\delta\mathcal{B}^{(k)} = -\sum_{i=1}^{m}\sum_{\ell=1}^{\rho_T} \mathcal{D}_{i,k}^{\ell^\top} X\Gamma Y^\top \mathcal{E}_{i,k}^{\ell^\top}$ the structured perturbation induced on matrix $\mathcal{B}$ of GEP (10), and with μ_ε^* the conjugate of μ_ε. Then we indicate with $(\delta A_k)_{p,q}$ the coefficient in position (p,q) of matrix δA_k, with $\mathcal{D}_{i,k}^{\ell,(p)}$ the p-*th* column of $\mathcal{D}_{i,k}^{\ell}$, and finally with $\mathcal{E}_{i,k,(q)}^{\ell}$ the q-*th* row of $\mathcal{E}_{i,k}^{\ell}$, for $p = 1,\dots,p_k,\ q = 1,\dots,q_k$.

From Lemma 1, using some algebraic manipulations, we obtain that

$$\frac{\partial|\mu_\varepsilon|^2}{\partial\delta A_k} = \left(\frac{\partial|\mu_\varepsilon|^2}{\partial(\delta A_k)_{p,q}}\right)_{\substack{p=1,\dots,p_k\\q=1,\dots,q_k}} = 2\Re\left(\mu_\varepsilon^* \frac{\partial\mu_\varepsilon}{\partial(\delta A_k)_{p,q}}\right)_{\substack{p=1,\dots,p_k\\q=1,\dots,q_k}} = 2\Re\left(\mu_\varepsilon^* \frac{x^*\frac{\partial\mathcal{B}}{\partial\delta A_k}y}{x^*\mathcal{A}y}\right)_{\substack{p=1,\dots,p_k\\q=1,\dots,q_k}} =$$
$$-\frac{2}{\xi}\sum_{i=1}^{m}\sum_{\ell=1}^{\rho_T}\Re\left(x^*\mathcal{D}_{i,k}^{\ell,(p)}\mathcal{E}_{i,k,(q)}y\mu_\varepsilon^*\right)_{\substack{p=1,\dots,p_k\\q=1,\dots,q_k}} = -\frac{2}{\xi}\sum_{i=1}^{m}\sum_{\ell=1}^{\rho_T}\left(\mathcal{D}_{i,k}^{\ell,(p)^\top}\Re\left(xy^*\mu_\varepsilon^*\right)\mathcal{E}_{i,k,(q)}^{\ell^\top}\right)_{\substack{p=1,\dots,p_k\\q=1,\dots,q_k}} =$$
$$-\frac{2}{\xi}\sum_{i=1}^{m}\sum_{\ell=1}^{\rho_T}\mathcal{D}_{i,k}^{\ell^\top}X\Gamma Y^\top\mathcal{E}_{i,k}^{\ell^\top}.$$

Since each δA_k is ε-bounded, the following constraint must hold,

$$g_k := \sum_{\substack{p=1,\dots,p_k\\q=1,\dots,q_k}}\left(\delta A_k\right)_{p,q}^2 - \varepsilon^2 \le 0, \quad k = 1,\dots,K.$$

As μ_ε has the globally largest modulus in the pseudospectrum, from the theory of Lagrange multipliers we have that

$$\frac{\partial|\mu_\varepsilon|^2}{\partial\delta A_k} - 2\lambda_k\delta A_k = 0, \quad k = 1,\dots,K,$$

where $\lambda_k \ge 0$ is the multiplier associated with the g_k inequality constraint. If $\sum_{i=1}^{m}\sum_{\ell=1}^{\rho_T}\mathcal{D}_{i,k}^{\ell^\top}X\Gamma Y^\top\mathcal{E}_{i,k}^{\ell^\top}$ is nonzero, then λ_k is strictly positive and g_k is an active constraint; therefore δA_k is a positive multiple of $\frac{\partial|\mu_\varepsilon|^2}{\partial\delta A_k}$ and from the condition $\left\|\delta A_k\right\|_F = \varepsilon$ we derive the thesis. □

In the last theorem we have proved the existence of some explicit formulas for the optimal perturbations when the norm constraint is active; these formulas could be employed as the fundamental step of a fixed point iteration (as done for instance to compute the pseudospectral abscissa of standard[29] and nonlinear[30] eigenvalue problems with complex-valued uncertainties). However, fixed point methods do not guarantee the monotonicity of the iterates. Therefore, as we will see in the following, the formulas provided by the theorem will only be used to initialize our algorithm for computing the Floquet pseudospectral radius. The latter is based on constructing a *steepest-ascent* differential equations on the matrix manifold

$$\{\Delta \in \mathbb{R}^* : \|\Delta\| \le \varepsilon\} = \left\{\Delta \in \mathbb{R}^* : \|\delta A_k\|_F \le \varepsilon,\ k = 1,\dots,K\right\}, \tag{28}$$

while it can also be interpreted as a continuous version of a proximal gradient method applied to (25).

The basic idea is to initialize perturbations $(\delta A_1,\dots,\delta A_K)$ on the GEP of the nominal system using formulas (27); then, we want to individuate a continuous and a.e. differentiable path on the manifold (28) along which the modulus of the largest eigenvalue is always non-decreasing. Assume for simplicity that a set of uncertainties Δ is depending in a continuous and a.e. differentiable manner on a real parameter γ, i.e., $\delta A_k = \delta A_k(\gamma)$ for $k = 1,\dots,K$. From now on, we will use "dot quantities" $(\delta\dot{A}_k)$ to refer to derivatives w.r.t. γ. Observe that maintaining the constraint $\left\|\delta A_k(\gamma)\right\|_F \le \varepsilon$ for all γ can be equivalently rephrased by putting the following restriction the rate of change: $\delta\dot{A}_k$ must be of the form

$$\delta\dot{A}_k(\gamma) = \begin{cases} R_k(\gamma) - \langle R_k(\gamma), \delta A_k(\gamma)\rangle\delta A_k(\gamma), & \text{if } \left\|\delta A_k(\gamma)\right\|_F = \varepsilon \text{ and } \langle R_k(\gamma), \delta A_k(\gamma)\rangle > 0,\\ R_k(\gamma), & \text{otherwise,}\end{cases} \tag{29}$$

where $R_k(\gamma) \in \mathbb{R}^{p_k\times q_k}$ is an arbitrary direction in the space of perturbations, while $\langle\cdot,\cdot\rangle$ stands for the Frobenius inner product. The reason why we have two separate cases is the constraint imposed on its norm. If $\left\|\delta A_k(\gamma)\right\|_F = \varepsilon$ and the intended direction of change, $R_k(\gamma)$, points outwards the ball $B_k = \{\delta A_k \in \mathbb{R}^{p_k\times q_k} : \left\|\delta A_k\right\|_F \le \varepsilon\}$, then following this direction would lead to a solution $\delta A_k(\gamma)$ such that $\left\|\delta A_k(\gamma+\eta)\right\|_F > \varepsilon$ for $\eta > 0$ sufficiently small, thus violating the constraint. This can be overcome by projecting $R_k(\gamma)$ on the tangent space to the ball. On the other hand, if direction $R_k(\gamma)$ points inwards the ball (or if $\left\|\delta A_k(\gamma)\right\|_F < \varepsilon$), then there is no need for a projection and any direction is allowd.

Now, it is clear that for each γ, the corresponding set $\Delta(\gamma) = \left(\delta A_1(\gamma),\dots,\delta A_K(\gamma)\right)$ defines a perturbation of the nominal system (1), and consequently a perturbed GEP (22). We want to define quantities $R_k(\gamma)$ in order to individuate a continuous and a.e. differentiable path along which the modulus of the largest eigenvalue of the perturbed GEP (22) is monotonically increasing. This direction is determined by considering the derivative of the modulus of an eigenvalue $\mu(\gamma)$ (with left eigenvector $x(\gamma)$ and

right eigenvector $y(\gamma)$ such that $x(\gamma)^* \mathcal{A} y(\gamma) > 0$) of the perturbed GEP w.r.t. parameter γ, which reads as

$$\frac{d|\mu(\gamma)|^2}{d\gamma} = 2\Re\left(\frac{x^*\left(\sum_{k=1}^{K} \frac{d\delta\mathcal{B}^{(k)}}{d\gamma}\right)\mu^* y}{x^*\mathcal{A}y}\right) = -\frac{2}{\xi}\Re\left(x^*\left(\sum_{k=1}^{K}\sum_{i=1}^{m}\sum_{\ell=1}^{\rho_T} \mathcal{D}_{i,k}^{\ell}\delta\dot{A}_k\mathcal{E}_{i,k}^{\ell}\right)\mu^* y\right),$$

where for simplicity of the notations we omitted the dependence of x and y on γ. Now substituting (29) in the last formula and assuming the easy case where $\delta\dot{A}_k = R_k$ we have

$$\frac{d|\mu(\gamma)|^2}{d\gamma} = -\frac{2}{\xi}\Re\left(x^*\left(\sum_{k=1}^{K}\sum_{i=1}^{m}\sum_{\ell=1}^{\rho_T} \mathcal{D}_{i,k}^{\ell}\delta\dot{A}_k\mathcal{E}_{i,k}^{\ell}\right)\mu^* y\right) = -\sum_{i=1}^{m}\sum_{k=1}^{K}\frac{2}{\xi}\left\langle X, \sum_{\ell=1}^{\rho_T}\mathcal{D}_{i,k}^{\ell}R_k\mathcal{E}_{i,k}^{\ell}Y\Gamma^\top\right\rangle =$$

$$= -\sum_{k=1}^{K}\frac{2}{\xi}\left\langle \sum_{i=1}^{m}\sum_{\ell=1}^{\rho_T}\mathcal{D}_{i,k}^{\ell^\top}X\Gamma Y^\top\mathcal{E}_{i,k}^{\ell^\top}, R_k\right\rangle$$

Therefore, the steepest ascent direction for $|\mu|$ is guaranteed by the choice

$$R_k = -\sum_{i=1}^{m}\sum_{\ell=1}^{\rho_T}\mathcal{D}_{i,k}^{\ell^\top}X\Gamma Y^\top\mathcal{E}_{i,k}^{\ell^\top}. \tag{30}$$

It is easy to see that up to the scaling by $2/\xi > 0$, choice (30) is nothing else than (the matriciation of the) gradient of objective function $|\mu|^2$ with respect to the elements of δA_k.

In the case where $\delta\dot{A}_k = R_k - \langle R_k, \delta A_k\rangle\delta A_k$ the same choice for R_k is used. It also leads to $\frac{d|\mu(\gamma)|^2}{d\gamma} \geq 0$, while the resulting direction $\delta\dot{A}_k$ can then be interpreted as the direction of the projected gradient on the tangent space to the set $\{\delta A_k : \|\delta A_k\|_F = \epsilon\}$. The latter is the steepest ascent direction among the feasible directions.

3.3 | Implementation

In the previous subsection we have established a continuous dependence of the set of matrix perturbations Δ on the parameter γ; for each γ we are able to individuate a steepest ascent direction for the modulus of the largest eigenvalue of the perturbed GEP (22): this direction is determined by ODEs (29) with choices (30) for $k = 1, \dots, K$. Therefore, the basic iteration of our algorithm works as follows: given some perturbed GEP, we pick its largest eigenvalue and follow an ascent direction for its modulus using equation (29) with R_k defined in (30); then, by applying forward Euler method with adaptive step size on the ODEs, we can define a novel perturbation such that the modulus of its largest eigenvalue has increased. We must stress here that the adaptive step size[22] employed in the forward Euler method guarantees the monotonicity of the modulus.

Observe also that at each iteration a projection of the newly obtained iterate on the ball B_k might be needed: for example if $\|\delta A_k\|_F = \epsilon$ and $\langle R_k, \delta A_k\rangle > 0$, then after the application of the Euler step the new iterate will not satisfy the norm constraint despite using the projected gradient as the curvature of the ball is not taken into account. Therefore, projection on B_k is necessary.

The algorithm is initialized using formulas (27) : these expressions could represent the basic operation of a fixed-point iteration; however, in terms of monotonicity of the iterates it is preferable to use a gradient-ascent method. Therefore, given an eigenvalue (and eigenvectors) of the nominal GEP, we first compute X, Y and Γ, and then we define the initial perturbations δA_k for $k = 1, \dots, K$ using (27). It is also important to highlight that the algorithm is restarted several times, where each time one among the largest eigenvalue of the nominal GEP is used for initialization.

The algorithm is stopped when the (projected) gradient of the modulus of the largest eigenvalue is below a prescribed tolerance; of course, being a gradient ascent method, this algorithm is not guaranteed to converge to the global maximum. However, the adaptive step size and the restarting strategy make it a very robust method to compute the globally largest eigenvalue (as already proved in the state-of-the-art methods used for computing the pseudospectral abscissa[29],[22]). Moreover, at each iteration we pick the largest eigenvalue and then proceed with the optimization of its modulus: this implies that the algorithm is able to switch from one targeted eigenvalue to another, if some non-targeted eigenvalue becomes the largest one at some point.

The whole structure of the method is illustrated in Algorithm 1.

Remark 1. It should be recalled that adding the uncertainty in (22) in every iteration step corresponds to updating the "snapshot" $A_i(\theta_T^{\ell})$ in (11) in accordance to (17), while matrices $\mathcal{D}_{i,k}^{\ell}, \mathcal{E}_{i,k}^{\ell}$ only need to be computed once.

Remark 2. In our algorithm constraints are implicitly addressed by projecting gradients and, in this way, restricting the generated path to the manifold (28) of feasible perturbations. Alternatively, generic nonlinear programming algorithms can be directly

applied to solve (25), with the explicit constraints $\delta A_k^T \delta A_k \leq \varepsilon,\ k = 1, \dots, K$ - recall that the gradient of the objective function can be constructed from (30). In such an approach there is no guarantee that all iterates are feasible.

4 | MODELS WITH PIECEWISE-CONTINUOUS PERIODIC FUNCTIONS

In this section we relax the conditions on functions A_i in (1) to $A_i \in \mathcal{R}_{\text{pws}}(T)^{n\times n}$, where

$$\mathcal{R}_{\text{pws}}(T) = \{f : \mathbb{R} \mapsto \mathbb{R} | f(t) = f(t+T)\ \forall\, t \in \mathbb{R}\ , f \text{ piecewise-continuous}\}.$$

To the best of our knowledge, the mathematical framework of Floquet theory (see, e.g., [10,9]) has not yet been extended to the case of piecewise-continuous coefficient matrices. However, in practice computing Floquet multipliers for TPDDEs with piecewise-continuous periodic functions has proven to be a reliable approach for assessing stability (see, for instance, [32,15]). From a numerical point of view, it is important to notice that at the time-instants of discontinuities in the coefficient matrices, the solutions of (1) exhibit discontinuities in their derivatives, which might negatively affect the convergence rate of (local) polynomial approximations. This problem can be addressed by ensuring that such time-instants correspond to boundary points of one of the intervals Ω_j, as in these points only continuity is imposed on the piecewise polynomial.

In Sections 4.1 and 4.2, we consider two popular examples of engineering applications modeled by piecewise-continuous TPDDEs. They concern the use of a delayed act-and-wait controller to stabilize a linear system and the milling problem, for which we provide an analysis of the stability robustness.

4.1 | Robustness analysis of linear systems stabilized by act-and-wait controllers

In this section we analyse the stability robustness of linear systems with delayed act-and-wait controller, which are characterized by the introduction of a piecewise-constant function [32]. In our numerical examples, we will consider a second-order model which is often used to analyse the stabilization of an inverted pendulum [25] and in applications such as human balancing problems [26].

The mechanical model of an inverted pendulum of length L and mass m driven on a massless cart is described by the linear system

$$\begin{cases} \dot{x}(t) = Ax(t) + Bu(t) \\ y(t) = Cx(t) \end{cases} \tag{31}$$

with state x, input u and output y, and

$$A = \begin{bmatrix} 0 & 1 \\ -\widetilde{a} & 0 \end{bmatrix},\ B = \begin{bmatrix} 0 \\ 1 \end{bmatrix},\ C = \begin{bmatrix} 1 & 0 \\ 0 & 1 \end{bmatrix},$$

where $\widetilde{a} = -3g/(6L)$. The controlled inverted pendulum represented in Figure 3a results from the coupling of system (31) with a time-periodic controller

$$u(t) = Dg(t)y(t-\tau), \tag{32}$$

where

$$D = \begin{bmatrix} -\widetilde{p} & -\widetilde{d} \end{bmatrix}$$

contains the control gains, τ is the time delay of the feedback loop, and g is a periodic function. The act-and-wait controller is a special case of time-periodic controllers, and we define the switching function g as follows

$$g(t) = \begin{cases} 0, \text{ if } 0 \leq (t \bmod T) < t_w, \\ 1, \text{ if } t_w \leq (t \bmod T) < t_w + t_a = T, \end{cases}$$

where t_w is the waiting period while the controller is not active, and t_a is the acting period while the controller is active.

Let us assume, for this specific example, that $t_w = 1.2\tau$ and $t_a = 0.8\tau$ (so that $T = 2\tau$). Thanks to these relations, we can introduce a transformation to work with a dimensionless time coordinate $\theta := t/\tau$. Then, our system (31) with controller (32) can be written in the same form for the dimensionless time coordinate θ, using the matrices

$$A = \begin{bmatrix} 0 & 1 \\ -a & 0 \end{bmatrix},\ B = \begin{bmatrix} 0 \\ 1 \end{bmatrix},\ C = \begin{bmatrix} 1 & 0 \\ 0 & 1 \end{bmatrix},\ D = \begin{bmatrix} -p & -d \end{bmatrix}, \tag{33}$$

where $a = \widetilde{a}\tau^2,\ p = \widetilde{p}\tau^2,\ d = \widetilde{d}\tau$, where $g(\theta)$ is now defined for $t_w = 1.2$ and $t_a = 0.8$, and finally the feedback delay τ is equal to one.

We want to show that an increase of the feedback delay in the original system determines a shrink of the stable and robustly stable domains. As a consequence of the time transformation, an increase of τ in (32) corresponds to an increase of the values of parameters $a,\ p,\ d$ in (33). In Figures 3b and 3c, we analyse the stability robustness for (33) considering $a = -2.5$ and $a = -3$, respectively. In both plots, we represent the stability boundary (outer line), the robust stability boundary for $|\delta a| \leq 0.02,\ |\delta p| \leq 0.05,\ |\delta d| \leq 0.05$ (middle line) and the robust stability boundary for $|\delta a| \leq 0.04,\ |\delta p| \leq 0.1,\ |\delta d| \leq 0.1$ (inner line).

It is readily observable that the increase of the feedback delay produces a shrink of the (robustly) stable regions. Firstly, we observe that for a larger a, the stable domain drifts and p, d assume larger values. Secondly, we see that the stable domain, and even more the robustly stable one, are characterized by a significant shrink.

Before we conclude, we would like to illustrate the *average* computational times for the calculation of the the stability and robust stability boundaries in Figure 3b (the computational times for Figure 3c are comparable). Here, we used a contour plotter on a grid of 80×80 points, and we have used a piecewise polynomial with degree $M = 40$. The time employed to compute the largest Floquet multiplier in each point is on average 0.07 seconds. Concerning the computation of the robust stability boundaries, it is clear that there is no reason to compute μ_ϵ for the points outside the stability region. Therefore, we averaged the computational times of Algorithm 1 only on the points inside the stability region: considering $n_{\text{start}} = 1$, a tolerance $\eta = 10^{-5}$ and a scaling factor $h = 2$ we have an average computational time of 2.89 and 2.88 seconds, for the middle green line and the inner red one, respectively. Observe that these times could be further reduced using a larger η or a larger h and, even more, these plots can be generated using parallel computing.

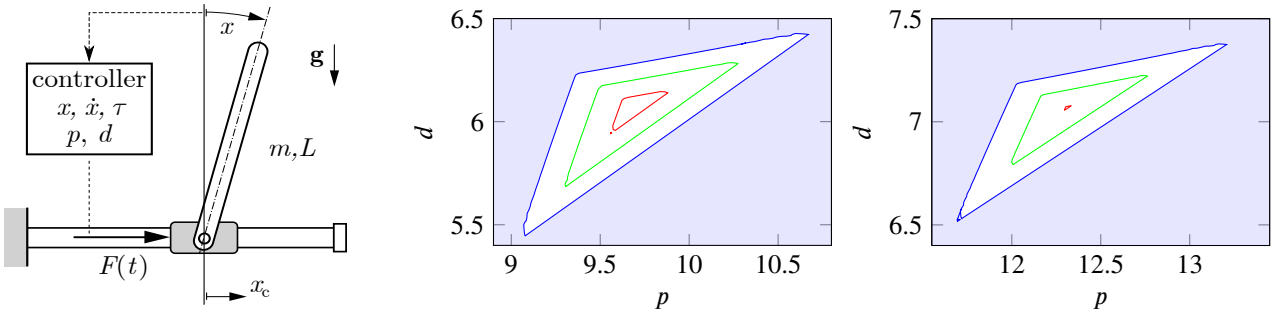

(a) **(b)** **(c)**

FIGURE 3 Panel (a) represents the mechanical model of an inverted pendulum (x_c is a cyclic coordinate that can be eliminated from the essential motion of the pendulum). Panels (b), (c) show the stability boundaries and the robust stability boundaries for system (31) controlled with (32): in (b) we consider $a = -2.5,\ t_w = 1.2,\ t_a = 0.8$, in (c) $a = -3,\ t_w = 1.2,\ t_a = 0.8$. In both cases, the middle (green) line shows the robust stability boundary for $|\delta a| \leq 0.02, |\delta p| \leq 0.05, |\delta d| \leq 0.05$, the inner (red) line for $|\delta a| \leq 0.04,\ |\delta p| \leq 0.1,\ |\delta d| \leq 0.1$. The shaded area represents the unstable region.

4.2 | Robustness analysis of milling operations

Manufacturing industry faces significant challenges in high speed cutting, because self-excited vibrations (called chatter) often arise during machining operations, such as milling and turning. These vibrations spoil the surface quality, increase the wear and reduce productivity. The evolution of the unstable vibrations are described by time-periodic DDEs, which originates from the so-called surface regeneration effect[33,34].

A dynamical model of a milling process is presented in Fig. 4, which describes the manufacturing operation of highly flexible workpieces, such as thin plates or turbine blades. The displacement of the workpiece is denoted by coordinate $y(t)$, while the radial and tangential forces $F_{j,\text{t}}$ and $F_{j,\text{r}}$ acting on tooth j ($j = 1, \ldots, Z$) are calculated from empirical models. The variational system given by coordinate $\eta(t)$ describes the behavior of the motion around the periodic solution $y_\text{p}(t)$, which reduces to the TPDDE in the form

$$m\ddot{\eta}(t) + c\dot{\eta}(t) + k\eta(t) = G(t)\big(\eta(t-\tau) - \eta(t)\big), \tag{34}$$

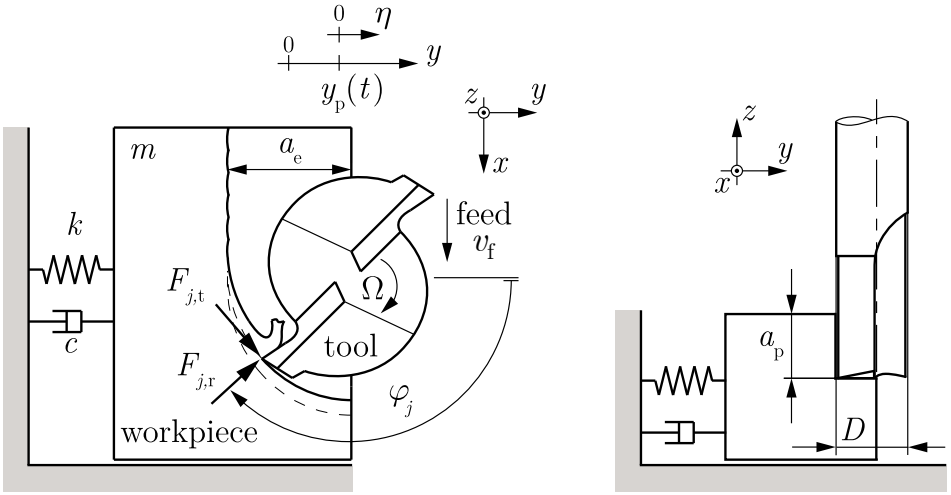

FIGURE 4 Dynamical model of milling in case of a single vibration mode.

where $\tau = 60/(Z\Omega)$ is the time delay, Ω is the spindle speed given in rpm, $G(t) = G(t+\tau)$ and m, c, k are modal parameters. The cutting force acting on tooth j at radial and tangential directions can be given by the formula $F_{j,d}(t) = a_p K_d h_j^q(t)$, $(d = \mathrm{t}, \mathrm{r})$, where K_t, K_r are cutting coefficients in tangential and radial directions, a_p is the axial depth of cut and $h_j(t)$ is the chip thickness. The periodic function $G(t)$ is then obtained in the form

$$G(t) = a_p q f_Z^{q-1} \sum_{j=1}^{Z} g_j(t)\big(-K_\mathrm{t}\sin\varphi_j(t) + K_\mathrm{r}\cos\varphi_j(t)\big)\cos\varphi_j(t)\sin^{q-1}\varphi_j(t), \tag{35}$$

where f_Z is the feed per tooth, $\varphi_j(t)$ gives the position of the cutting edge as

$$\varphi_j(t) = \frac{2\pi\Omega}{60}t + j\frac{2\pi}{Z}, \tag{36}$$

and

$$g_j(t) = \begin{cases} 1, & \text{if } \varphi_{\mathrm{en}} < (\varphi_j(t) \bmod 2\pi) < \varphi_{\mathrm{ex}}, \\ 0, & \text{otherwise}, \end{cases} \tag{37}$$

is an indicator function determining whether the edge is in contact with the material or not. Here, φ_{en} and φ_{ex} denote the entering and exiting angles of the cutting edges. More details on the topic can be found in [35] or [12].

A stability diagram is visualized in the plane of spindle speed Ω and depth of cut a_p. In Fig. 5 the nominal stability boundaries were calculated using the parameters $m = 1$ kg, $c = 40$ Ns/m, $k = 10^6$ N/m, $q = 3/4$, $K_\mathrm{t} = 800$ N/m^{1+q}, $K_\mathrm{r} = 300$ N/m^{1+q}, $f_Z = 0.1$ mm/tooth, $Z = 2$, $D = 16$ mm, $a_e = 2$ mm, and the operation was upmilling with $\varphi_{\mathrm{en}} = 0°$, $\varphi_{\mathrm{ex}} = 41.41°$. The cutting parameters K_t and K_r are usually determined from preliminary cutting tests, and their uncertainty can be significant. Robust stability diagrams were calculated assuming 10 % (or 20%) relative uncertainty in these two parameters, i.e., $|\delta K_\mathrm{t}| < 0.1K_\mathrm{t}$ and $|\delta K_\mathrm{r}| < 0.1K_\mathrm{r}$ (or $|\delta K_\mathrm{t}| < 0.2K_\mathrm{t}$ and $|\delta K_\mathrm{r}| < 0.2K_\mathrm{r}$). The scaling matrices of the uncertainty are periodic in the pseudospectral method. The results clearly show that the uncertainty affects the regions of the stable domain in different extent.

Also in this case, we report the computational times for the generation of Figure 5. We used a contour plotter on a grid of 90×150 points, and used a piecewise polynomial approximation with degree $M = 30$. For each point of the grid, the computation of the largest Floquet multiplier of the corresponding system took *an average* of 0.05 seconds. On those points characterizing a stable configuration, we then computed the Floquet pseudospectral radius μ_ϵ running Algorithm 1 for $n_{\mathrm{start}} = 3$, $\eta = 10^{-5}$ and $h = 2$; we observed an *average* running time of 6.70 and 6.39 seconds for the robust stability boundaries corresponding to a 10% and a 20% uncertainty on K_t and K_r, respectively. Another application of the pseudospectral approach to milling is described in [36], where numerical computations are tested against experimental results.

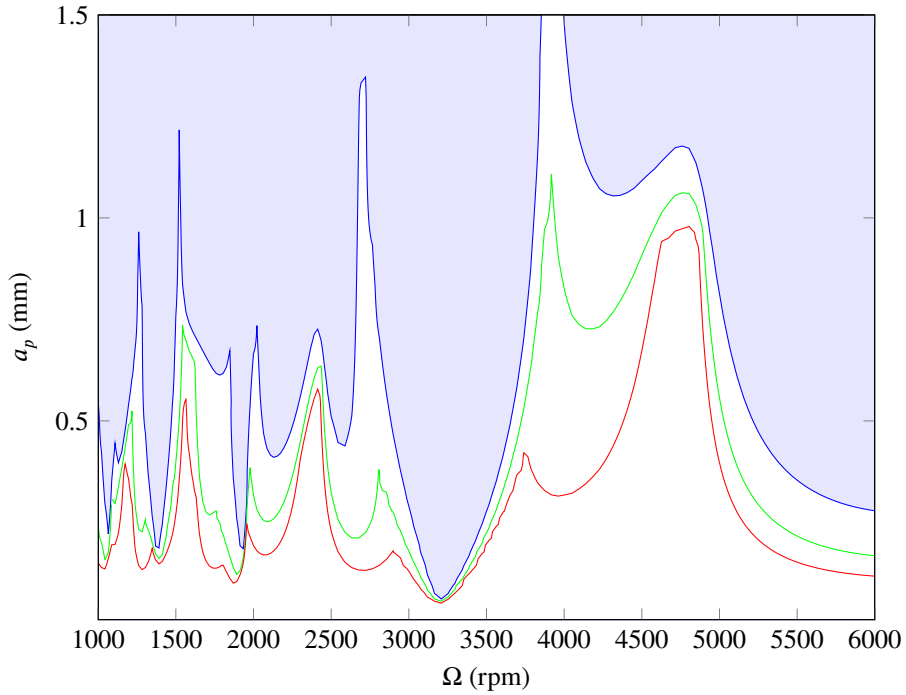

FIGURE 5 Robust stability diagram: the upper (blue) line is the stability boundary, the middle (green) line is the robust stability boundary for 10% relative uncertainty in K_t, K_r and the lower (red) line is the robust stability boundary for 20% relative uncertainty in K_t, K_r; the shaded area is the unstable region.

5 | MODELS WITH PERIODICALLY TIME-VARYING DELAYS

Another main application which can be tackled with (a slight extension of) our method is the robust stability analysis of a turning operation with spindle speed variation, which is commonly described by TPDDEs with smooth periodic functions and periodically-varying delays.

If the delays in (1) are not constant but time-periodic functions, $\tau_i \in \mathcal{R}(T)$, satisfying $0 \leq \tau_1(t) < \cdots < \tau_m(t)$, the only adaptation the algorithms presented in Sections 2-3 consists of defining $\tau_{\max} := \tau_m(0)$, and replacing conditions (11) by

$$\left(\mathcal{I}^{(1)}(\theta_T^\ell) - \sum_{i=1}^{m} A_i(\theta_T^\ell) \mathcal{I}^{(0)} \left(\theta_T^\ell - \tau_i(\theta_T^\ell) \right) \right) \vec{C} = 0, \quad \text{for each } \theta_T^\ell \in m_T.$$

Regarding the mathematical foundations, it is demonstrated in[37] that if there is one delay $\tau(t)$ such that the function

$$t \mapsto \tau(t)$$

is invertible, which is satisfied if $\dot{\tau}(t) < \rho$, with $\rho < 1$, then there always an (invertible) time- transformation resulting in a system with constant delay. This property allows to directly extend the Floquet theory and justifies the computation of Floquet multipliers for stability assessment.

5.1 | Robustness analysis of spindle speed variation in turning

Machine tool chatter is a challenging problem in turning operations, too. A well-known method to suppress vibrations during turning processes is spindle speed variation. The main idea behind this concept is that spindle speed variation introduces a time-varying regenerative delay, which in some cases may stabilize the process. The dynamical model of a turning operation is presented in Fig. 6. The regenerative time delay in case of constant speed (Ω_0) is simply given as $\tau_0 = 60/\Omega_0$. On the other hand, in the case of a time-varying spindle speed, we assume that the speed is modulated around the nominal value as

$$\Omega(t) = \Omega_0 + S(t)\Omega_1, \tag{38}$$

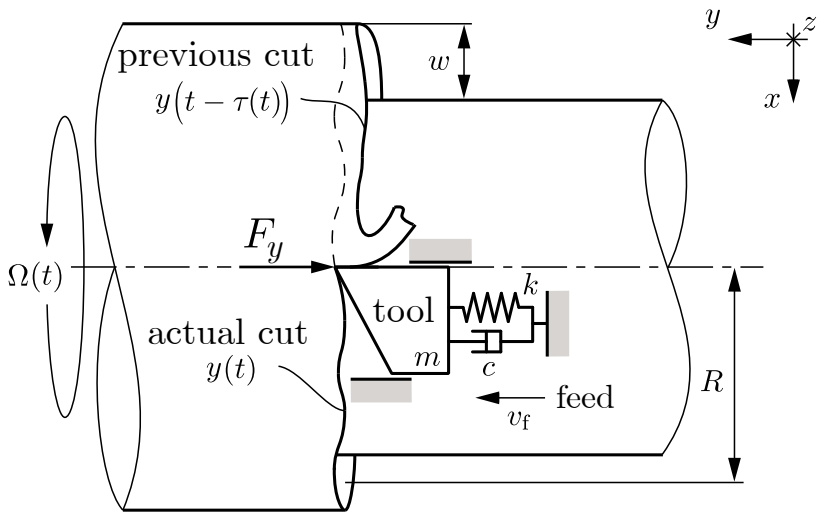

FIGURE 6 Dynamical model of spindle speed variation in turning.

where Ω_1 is the amplitude of the harmonic variation $S(t) = \cos(2\pi t/T)$ defined as $\Omega_1 = (\mathrm{RVA})\Omega_0$ for some RVA $\in \mathbb{R}^+$ (observe that the coefficient RVA can be interpreted as the ratio between the amplitude of the harmonic variation Ω_1 and the mean spindle speed Ω_0). For simplicity, the time delay is then approximated by the relation

$$\tau(t) \approx \tau_0 - S(t)\tau_1, \quad \tau(t+T) = \tau(t), \tag{39}$$

where again τ_1 is the amplitude of the harmonic variation $S(t)$ and such that $\tau_1 := (\mathrm{RVA})\tau_0$.

Similarly, the ratio of the average time delay τ_0 and the period is set equal to a real-valued parameter RVF $:= \tau_0/T$.

The governing equation of the turning process can be given as

$$m\ddot{\eta}(t) + c\dot{\eta}(t) + k\eta(t) = G(t)\Big(\eta\big(t-\tau(t)\big) - \eta(t)\Big), \quad G(t) = wK_y q(v_\mathrm{f}\tau_0)^{q-1}\left(\frac{\tau(t)}{\tau_0}\right)^{q-1}, \tag{40}$$

where $G(t+T) = G(t)$ is a periodic function, moreover m, c and k are modal parameters, w is the depth of cut, $h_0 := v_\mathrm{f}\tau_0$ is the theoretical prescribed chip thickness, q and K_y are cutting parameters. For more details on the model, see [12].

A stability diagram is visualized in the plane of mean spindle speed Ω_0 and depth of cut w, while RVA and RVF are fixed. In Fig. 7 the nominal stability boundaries were calculated using the parameters $m = 1$ kg, $c = 40$ Ns/m, $k = 10^6$ N/m, $q = 3/4$, $K_y = 300$ N/m^{1+q}, $h_0 = 0.1$ mm. In (a) RVA=0, i.e., spindle speed variation is off, therefore it gives the unmodulated constant speed turning model. In (b) we set RVA=0.1 and RVF=0.5: it is easy to check that with this choice of values the condition $\dot{\tau}(t) < 1$ is satisfied for all $t \in [0, T]$. In both cases we assume that modal damping c and modal stiffness k are uncertain, and we set $|\delta k| < 0.05k$ and $|\delta c| < 0.4c$. Since the relative damping ratio ($\zeta = c/(2\sqrt{km}) = 2\%$) is small, 40% uncertainty results damping ratio between 1.2-2.8%, which is still in the reasonable range. As it is seen from Fig. 7 (a) and (b), the robustness of spindle speed variation at different speeds might significantly affect the selection of optimal machining parameters.

We provide here the computational times for the generation of Figure 7(b). We used a contour plotter on a grid of 40×60 points, and we have approximated the solution with a piecewise polynomial with degree $M = 80$. The computation of the largest Floquet multiplier for the system defined by each grid point took *on average* 0.12 seconds. The pseudospectral radius was computed in the points defining a *stable* configuration for the corresponding nominal system: for each of these points, we ran Algorithm 1 for $n_{\mathrm{start}} = 2$ (using the two largest Floquet multipliers of the unperturbed system as initial values), $\eta = 10^{-5}$ and $h = 2$, observing an *average* computational time of 9.03 seconds.

6 | CONCLUSIONS

We presented, to the best of the authors' knowledge, the first Floquet multipliers-based method to assess the stability robustness of a system of time-periodic delay differential equations: the method computes the largest Floquet multiplier arising within a class of real-valued structured perturbations on the coefficient matrices A_i, and it is not conservative as it is grounded on a necessary

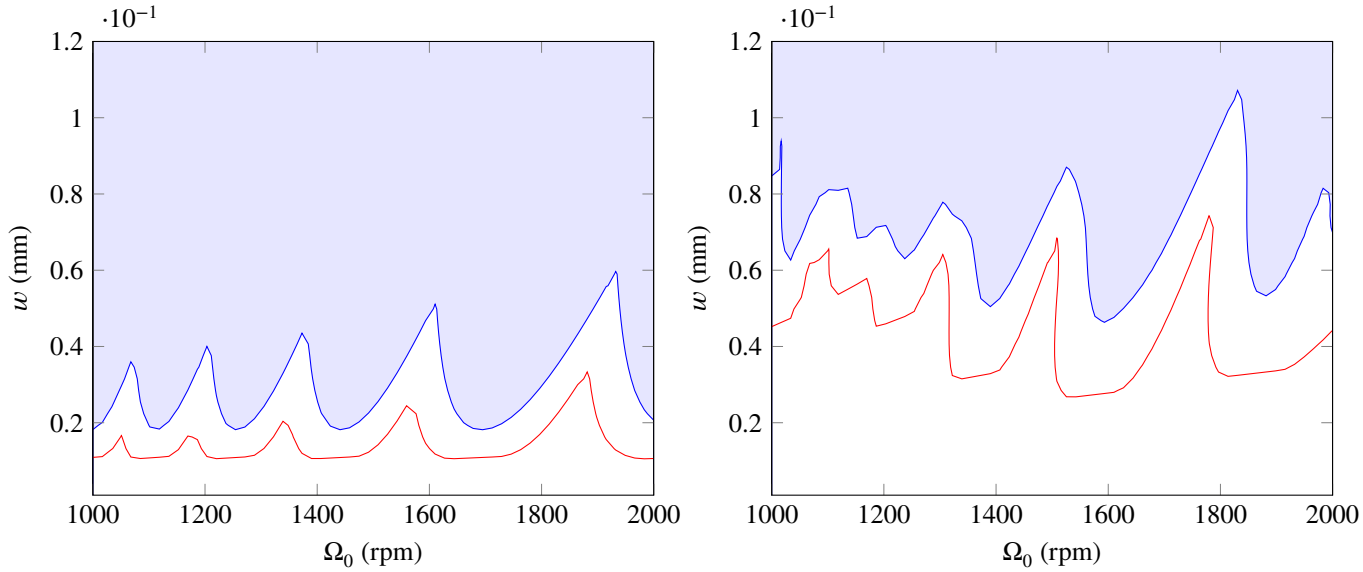

FIGURE 7 Robust stability diagram: the upper (blue) line is the stability boundary, the lower (red) line is the robust stability boundary for $|\delta k| < 0.05k$, $|\delta c| < 0.4c$. In panel (a) we set RVA=0, in panel (b) we set RVA=0.1 and RVF=0.5.

and sufficient condition for the stability robustness. The uncertainties can be considered as either constant or periodically-varying as well. The method deals with TPDDEs with discontinuous periodic functions and with TPDDEs with periodically-varying delays, which are very common in engineering applications: examples and numerical simulations are presented for an inverted pendulum subject to an act-and-wait controller, for a single-degree-of-freedom milling model and for a turning operation with spindle speed variation. Instrumental to the approach was a spectral collocation scheme for computing Floquet multipliers, which results in a generalized eigenvalue problem where the coefficient matrices have affine dependence on the uncertainty.

Future work includes the extension of the approach toward TPDDEs exhibiting combined uncertainty on coefficient matrices, delays or period. For the special case where the ratios between delays and period are invariant, the presented approach might still be applicable using a preliminary time-transformation, as we have seen in Section 4.1.

ACKNOWLEDGMENTS

The authors thank the anonymous reviewers for the careful reading and constructive comments that significantly improved the paper.

This research was supported by the project C14/17/072 of the KU Leuven Research Council, by the project G0A5317N of the Research Foundation Flanders (FWO - Vlaanderen), by the National Research, Development and Innovation Fund (TUDFO/51757/2019-ITM, Thematic Excellence Program), by the Higher Education Excellence Program of the Ministry of Human Capacities in the frame of Artificial intelligence research area of Budapest University of Technology and Economics (BME FIKP-MI), and by the Hungarian Scientific Research Fund OTKA FK-124462.

References

1. Insperger T, Mann B, Stépán G, Bayly P. Stability of up-milling and down-milling, part 1: alternative analytical methods. *Int J Mach Tool Manu* 2003; 43(1): 25-34.

2. Totis G, Insperger T, Sortino M, Stépán G. Symmetry breaking in milling dynamics. *Int J Mach Tool Manu* 2019; 139: 37-56.

3. Insperger T, Kovács L, Galambos P, Stépán G. Increasing the accuracy of digital force control process using the act-and-wait concept. *IEEE/ASME T Mech* 2010; 15(2): 291-298.

4. Hagan M, Demuth H, Beale M, De Jesús O. *Neural network design (2nd Edition)*. Boston: Martin Hagan . 2014.

5. Deshmukh V, Ma H, Butcher E. Optimal control of parametrically excited linear delay differential systems via Chebyshev polynomials. *Optim. Control Appl. Meth.* 2006; 27: 123-136.

6. Michiels W, Niculescu S. *Stability and stabilization of time-delay systems. An eigenvalue based approach*. SIAM . 2007.

7. Gu K, Kharitonov V, Chen J. *Stability of time-delay systems*. Birkhauser . 2003.

8. Farkas M. *Periodic Motions*. Springer-Verlag, New York . 1994.

9. Diekmann O, Van Gils S, Verduyn Lunel S, Walther H. *Delay equations–functional, complex and nonlinear analysis*. New-York: Springer . 1995.

10. Hale J. *Theory of functional differential equations*. New-York: Springer . 1977.

11. Breda D, Maset S, Vermiglio R. *Stability of linear delay differential equations: a numerical approach with MATLAB*. Springer-Verlag . 2015.

12. Insperger T, Stépán G. *Semi-Discretization for Time-Delay Systems*. New-York: Springer–Verlag . 2011.

13. Insperger T, Stépán G. Semi-discretization method for delayed systems. *Int J Numer Meth Eng* 2002; 55(5): 503-518.

14. Khasawneh F, Mann B. A spectral element approach for the stability analysis of time-periodic delay equations with multiple delays. *Commun Nonlinear Sci Numer Simulat* 2013; 18: 2129-2141.

15. Lehotzky D, Insperger T, Khasawneh F, Stépán G. Spectral element method for stability analysis of milling processes with discontinuous time-periodicity. *Int J Adv Manuf Technol* 2017; 89: 2503-2514.

16. DDE-Biftool implementation. Available from `sourceforge.net/p/ddebiftool/git/ci/master/tree/`; .

17. Butcher E, Ma H, Bueler E, Averina V, Szabo Z. Stability of linear time-periodic delay-differential equations via Chebyshev polynomials. *Int J Numer Meth Eng* 2004; 59: 895-922.

18. Letyagina O, Zhabko A. Robust stability analysis of linear periodic systems with delay. *Int. J. Mod. Phys. A* 2009; 24(5): 893-907.

19. De Souza C, Coutinho D. Stability of Linear Discrete-Time Periodic Systems with Time-Delay. In: Proc. 4th IFAC international workshop on periodic control systems. ; August 26–28, 2010; Antalya, Turkey.

20. De Souza C, Coutinho D. Robust stability and control of uncertain linear discrete-time periodic systems with time-delay. *Automatica* 2013; 50: 431-441.

21. Koch O, Lubich C. Dynamical low rank approximation. *SIAM J. Matrix Anal. Appl.* 2007; 29(2): 434-454.

22. Guglielmi N, Lubich C. Low-rank dynamics for computing extremal points of real pseudospectra. *SIAM Journal of Matrix Analysis and Applications* 2013; 34: 40-66.

23. Borgioli F, Michiels W. A Novel Method to Compute the Structured Distance to Instability for Combined Uncertainties on Delays and System Matrices. *IEEE T. Automat. Contr.* 2019. DOI: 10.1109/TAC.2019.2934182.

24. Available from `http://twr.cs.kuleuven.be/research/software/delay-control/PDDE`; .

25. Stepan G. *Retarded dynamical systems*. Longman, Harlow, UK . 1989.

26. Milton J, Cabrera J, Ohira T, et al. The time-delayed inverted pendulum: implications for human balance control. *CHAOS 19* 2009. Article No. 026110.

27. Dankowicz H, Schilder F. *Recipes for continuation*. SIAM . 2013.

28. Insperger T, Stépán G. Stability chart for the delayed Mathieu equation. In: . 458 of *Proc. of the Royal Society A*. ; 2002: 1989-1998.

29. Guglielmi N, Overton M. Fast algorithms for the approximation of the pseudospectral abscissa and pseudospectral radius of a matrix. *SIAM Journal on Matrix Analysis and Applications* 2011; 32: 1166-1192.

30. Michiels W, Guglielmi N. An iterative method for computing the pseudospectral abscissa for a class of nonlinear eigenvalue problems. *SIAM Journal on Scientific Computing* 2012; 34(4): A2366-A2393.

31. Schreiber K. *Nonlinear eigenvalue problems: Newton-type methods and nonlinear Rayleigh functionals*. PhD thesis. TU Berlin, 2008.

32. Insperger T, Stépán G. On the dimension reduction of systems with feedback delay by act-and-wait control. *IMA J Math Control Inform* 2010; 27(4): 457-473.

33. Tobias SA. *Machine-tool Vibration*. Glasgow: Blackie . 1965.

34. Tlusty J, Spacek L. *Self-excited vibrations on machine tools*. Prague. in Czech.: Nakl. CSAV . 1954.

35. Altintas Y. *Manufacturing Automation: Metal Cutting Mechanics, Machine Tool Vibrations, and CNC Design*. Cambridge University Press. 2 ed. 2012

36. Hajdu D, Borgioli F, Michiels W, Insperger T, Stépán G. Robust stability of milling operations based on pseudospectral approach. *Int. J. Mach. Tool Manu.* 2020. DOI: 10.1016/j.ijmachtools.2019.103516.

37. Verriest E. Well-posedness of Problems involving Time-varying Delays. In: Proceedings of the 19th International Symposium on Mathematical Theory of Networks and Systems. ; July 5–9, 2010; Budapest, Hungary.

APPENDIX

In this Appendix we provide implementation details of the software for the Floquet multipliers computation which we made publicly available[24]. In addition, we explicitly state the GEP (10) in the easy case where $A_i \in \mathcal{R}(T)$, time delays are constant and $T > \tau_{\max}$.

Let us consider the system (1), and let us assume that matrices $A_i,\ i = 1, \dots, m$ admit a finite set of discontinuity points $\{P_1, \dots, P_H\}$ disposed in decreasing order, i.e., $0 < P_H < \dots < P_1 < T$. This peculiar choice about the order of points P_j is necessary in order to be consistent with the notation on subintervals Ω_j introduced in Section 2. Then, we subdivide the interval $[0, T]$ into a set of $H + 1$ subintervals Ω_j as follows

$$[0, T] = \bigcup_{j=0}^{H} \Omega_{H+1-j} = \bigcup_{j=0}^{H} [P_{H+1-j}, P_{H-j}], \quad \text{where } P_{H+1} = 0,\ P_0 = T.$$

The reason for the adopted discretization is that the solution x of (1) is continuous but non-differentiable in points $P_1, \dots, P_H$. Moreover, as a consequence of the definition of an eigenfunction and in particular of (9), the points of non-differentiability must be propagated to the subdomain $[-\tau_{\max}, 0]$ as well. In this description we assume that there exists $Q \in \mathbb{N}$ such that $QT < \tau_{\max} < (Q + 1)T$; moreover, we assume that $P_{q+1} - (Q + 1)T < \tau_{\max} < P_q - (Q + 1)T$ for some $q \in 0, \dots, H$. Then the interval $[-\tau_{\max}, T]$ is divided into $N = (Q + 1)(H + 1) + (q + 1)$ subintervals as illustrated in Figure 1. Observe that the considered case is a generalization of the easier condition where $\tau_{\max} = QT$ for some $Q \geq 1$. If the coefficients of the matrices A_i are continuous functions, we adopt a simpler discretization like the one highlighted in red in Figure 1. Assuming again that there exists $Q \in \mathbb{N}$ such that $QT < \tau_{\max} < (Q + 1)T$, we then set $\Omega_1 = [0, T], \Omega_j = [-(j - 1)T, -(j - 2)T]$ for $j = 2, \dots, Q + 1$

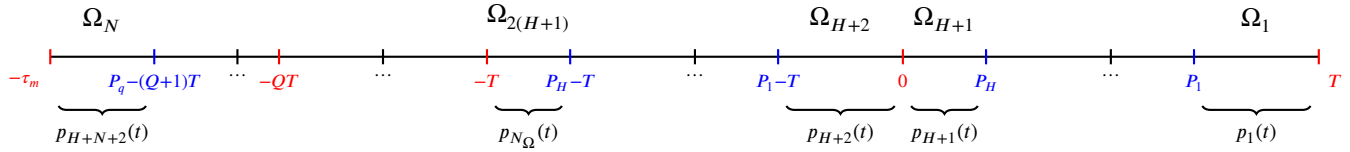

FIGURE 1 Discretization of the domain $[-\tau_m, T]$ for the system of TPDDE (1). Points colored in red are also present in the discretization of the domain adopted for TPDDEs with continuous terms. Points colored in blue are introduced in the discretization in order to handle (potential) discontinuities. Solution x of (1) is non-differentiable in the blue points.

and finally $\Omega_N = \Omega_{Q+2} = [-\tau_{\max}, -QT]$.

Given a discretization of the domain $[-\tau_{\max}, T]$, on the subintervals Ω_j we define a set of non-overlapping grids of Chebyshev-distributed points; let us consider a generic mesh of Chebyshev-distributed points $\alpha := \{\alpha^\ell\}_{\ell=1,\dots,M+1}$ defined on the interval $[-1, 1]$, where

$$\alpha^\ell = -\cos\left(\frac{\pi\ell}{M+1}\right), \quad \text{for } \ell = 1, \dots, M+1. \tag{1}$$

If we write each interval $\Omega_j = [a_j, b_j]$ for $j = 1, \dots, N$, then we can easily define a mesh of Chebyshev-distributed points on each Ω_j by applying the following transformations on the mesh points α^ℓ

$$\theta_j^\ell = f_j(\alpha^\ell) := \frac{1}{2}(a_j + b_j) + \frac{\alpha^\ell}{2}(b_j - a_j), \quad \text{for } \begin{cases} \ell = 1, \dots, M+1, \text{ if } \Omega_j \subset [-\tau_{\max}, 0], \\ \ell = 1, \dots, M, \text{ if } \Omega_j \subset [0, T], \end{cases} \tag{2}$$

and whose inverse transformations reads

$$\alpha^\ell = g_j(\theta_j^\ell) = \left(\theta_j^\ell - \frac{1}{2}(a_j + b_j)\right)\frac{2}{b_j - a_j}, \quad \text{for } \begin{cases} \ell = 1, \dots, M+1, \text{ if } \Omega_j \subset [-\tau_{\max}, 0], \\ \ell = 1, \dots, M, \text{ if } \Omega_j \subset [0, T]. \end{cases} \tag{3}$$

The different number of points adopted is due to the non-overlapping grids adopted, and to the fact that we want each p_j to have degree M: to this purpose, we will impose continuity on the boundary points of subintervals $\Omega_j \subset [0, T]$.

In our implementation, we construct each p_j using a basis of Chebyshev polynomials of the first kind; the choice of the Chebyshev polynomials rather than some other basis lies in the numerical stability.

In what follows, we provide details of our implementation using a basis of Chebyshev polynomials, and write explicit forms for the matrices defining the GEP (10). In particular, we will go through the three kinds of conditions imposed in Section 2 to construct (10) considering the following easy case:

$$\dot{x}(t) = \sum_{i=1}^{m} A_i(t)x(t - \tau_i), \tag{4}$$

where $A_i \in \mathcal{R}(T)^{n\times n}$, the time delays are constant and $T > \tau_m =: \tau_{\max}$. We then define here only two subintervals Ω_j, with $\Omega_1 = [0, T]$ and $\Omega_2 = [-\tau_{\max}, 0]$.

- We consider the collocation constraints for equation (9), thus we have

$$\mu p(\theta_2^\ell) = p(\theta_2^\ell + T), \text{ for } \ell = 1, \dots, M+1,$$

whose explicit form for (13) (that involves the interpolation operator) reads as

$$\mu \Big[T_0(\alpha^\ell) \otimes I_n \ \dots \ T_M(\alpha^\ell) \otimes I_n \overbrace{0 \otimes I_n \ \dots \ 0 \otimes I_n}^{n\times(M+1)\text{ columns}}\Big]\vec{C} =$$

$$\Big[\overbrace{0 \otimes I_n \ \dots \ 0 \otimes I_n}^{n\times(M+1)\text{ columns}} T_0\left(g_1(\theta_2^\ell + T)\right) \otimes I_n \ \dots \ T_M\left(g_1(\theta_2^\ell + T)\right) \otimes I_n\Big]\vec{C}.$$

Note that we exploit the hypothesis that $T > \tau_{\max}$, which guarantees that $\theta_2^\ell + T \in \Omega_1$ for each $\ell = 1, \dots, M+1$.

- Since we only have two intervals, the continuity of p must be imposed only for $t = 0$: the condition $p_1(0) = p_2(0)$ has the following matricial form

$$I_n \otimes \left[T_0(1) \ \dots \ T_M(1) \ -T_0(-1) \ \dots \ -T_M(-1) \right] \vec{C} = 0.$$

- We finally consider the collocation constraints for the TPDDE (4): we recall here that the Chebyshev polynomial of the second kind U_s with degree s is such that $\dot{T}_s(t) = sU_{s-1}(t)$. In order to correctly impose the condition, here we must carefully check whether the point $t - \tau_i$ falls in Ω_1 or in Ω_2. Then, for each θ_1^ℓ we consider the index m_ℓ s.t. $\theta_2^\ell \geq \tau_i$ for $i = 1, \dots, m_\ell$, and $\theta_1^\ell < \tau_i$ for $i = m_\ell + 1, \dots, m$. Observing that $g_1'(t) = 2/T$, equation (11) can be recast in the following matricial form for each $\ell = 1, \dots, M$

$$\left[\overbrace{0 \otimes I_n \ \dots \ 0 \otimes I_n}^{n \times (M+1) \text{ columns}} \ 0 \otimes I_n \ \tfrac{2}{T} U_0\left(\alpha^\ell\right) \otimes I_n \ \dots \ \tfrac{2}{T} M U_{M-1}\left(\alpha^\ell\right) \otimes I_n \right] \vec{C} -$$

$$\left[\overbrace{0 \otimes I_n \ \dots \ 0 \otimes I_n}^{n \times (M+1) \text{ columns}} \ \sum_{i=1}^{m_\ell} A_i(\theta_1^\ell) T_0\left(g_1(\theta_1^\ell - \tau_i)\right) \ \dots \ \sum_{i=1}^{m_\ell} A_i(\theta_1^\ell) \overbrace{T_M\left(g_1(\theta_1^\ell - \tau_i)\right)}^{n \times (M+1) \text{ columns}} \right] \vec{C} -$$

$$\left[\sum_{i=m_\ell+1}^{m} A_i(\theta_1^\ell) T_0\left(g_2(\theta_1^\ell - \tau_i)\right) \ \dots \ \sum_{i=m_\ell+1}^{m} A_i(\theta_1^\ell) T_{M-1}\left(g_2(\theta_1^\ell - \tau_i)\right) \ \overbrace{0 \otimes I_n \ \dots \ 0 \otimes I_n}^{} \right] \vec{C} = 0.$$

  Of course, there exist two limit cases: if $\theta_\ell^{(1)} < \tau_i$ for all $i = 1, \dots, m$, then $m_\ell = 0$ and the second term on the left-hand side does not appear; on the other hand, if $\theta_\ell^{(1)} \geq \tau_i$ for all $i = 1, \dots, m$, then $m_\ell = m$ and the third term is not needed.

Putting all the equations together, we have these explicit forms for $\mathcal{A}$ and $\mathcal{B}$:

$$\mathcal{A} := \begin{bmatrix} \mathcal{I}^{(0)}(m_\tau) \\ 0_{n(M+1) \times N_{eqn}} \end{bmatrix} \quad \text{with } \mathcal{I}^{(0)}(m_\tau) = \left[\begin{array}{ccc|c} T_0(\alpha^1) \otimes I_n & \dots & T_M(\alpha^1) \otimes I_n & \\ \vdots & \vdots & \vdots & 0_{n(M+1) \times n(M+1)} \\ T_0(\alpha^{M+1}) \otimes I_n & \dots & T_M(\alpha^{M+1}) \otimes I_n & \end{array} \right],$$

$$\mathcal{B} := \begin{bmatrix} \mathcal{I}^{(0)}(m_\tau + T) \\ M_1 \end{bmatrix} = \mathcal{B}_1 - \mathcal{B}_2 = \left[\frac{\mathcal{I}^{(0)}(m_\tau + T)}{\mathcal{B}_1^{(b)}} \right] - \left[\frac{0_{n(M+1) \times N_{\text{eqn}}}}{B_2^{(l)} \mid B_2^{(r)}} \right],$$

with

$$\mathcal{I}^{(0)}(m_\tau + T) = \left[0_{n(M+1) \times n(M+1)} \left| \begin{array}{ccc} T_0\left(g_1(\theta_2^1 + T)\right) \otimes I_n & \dots & T_M\left(g_1(\theta_2^1 + T)\right) \otimes I_n \\ \vdots & \vdots & \vdots \\ T_0\left(g_1(\theta_2^{M+1} + T)\right) \otimes I_n & \dots & T_M\left(g_1(\theta_2^{M+1} + T)\right) \otimes I_n \end{array} \right. \right],$$

$$\mathcal{B}_1^{(b)} := \left[\frac{0 \otimes I_n \quad \dots \quad 0 \otimes I_n}{\mathcal{I}^{(1)}(m_T)} \right], \text{ with } \mathcal{I}^{(1)}(m_T) = \left[0_{nM \times n(M+2)} \left| \begin{array}{ccc} \frac{2}{T} U_0\left(\alpha^1\right) \otimes I_n & \dots & \frac{2}{T} M U_{M-1}\left(\alpha^1\right) \otimes I_n \\ \vdots & \vdots & \vdots \\ \frac{2}{T} U_0\left(\alpha^M\right) \otimes I_n & \dots & \frac{2}{T} M U_{M-1}\left(\alpha^M\right) \otimes I_n \end{array} \right. \right],$$

$$B_2^{(l)} := \begin{bmatrix} I_n \otimes T_0(1) & \dots & I_n \otimes T_M(1) \\ \sum_{i=m_1+1}^{m} A_i(\theta_1^1) T_0\left(g_2(\theta_1^1 - \tau_i)\right) & \dots & \sum_{i=m_1+1}^{m} A_i(\theta_1^1) T_M\left(g_2(\theta_1^1 - \tau_i)\right) \\ \vdots & \vdots & \vdots \\ \sum_{i=m_M+1}^{m} A_i(\theta_1^M) T_0\left(g_2(\theta_1^M - \tau_i)\right) & \dots & \sum_{i=m_M+1}^{m} A_i(\theta_1^M) T_M\left(g_2(\theta_1^M - \tau_i)\right) \end{bmatrix},$$

$$B_2^{(r)} := \begin{bmatrix} -I_n \otimes T_0(-1) & \dots & -I_n \otimes T_M(-1) \\ \sum_{i=1}^{m_1} A_i(\theta_1^1) T_0\left(g_1(\theta_1^1 - \tau_i)\right) & \dots & \sum_{i=0}^{m_1} A_i(\theta_1^1) T_M\left(g_1(\theta_1^1 - \tau_i)\right) \\ \vdots & \vdots & \vdots \\ \sum_{i=1}^{m_M} A_i(\theta_1^M) T_0\left(g_1(\theta_1^M - \tau_i)\right) & \dots & \sum_{i=0}^{m_M} A_i(\theta_1^M) T_M\left(g_1(\theta_1^M - \tau_i)\right) \end{bmatrix}.$$

In what follows, for the same case we also provide explicit expressions for matrices $\mathcal{D}^{\ell}_{i,k}$, $\mathcal{E}^{\ell}_{i,k}$ introduced at the beginning of subsection 3.1.1; we then need to impose $M+1$ collocation conditions for equation (9) plus the continuity condition imposed in 0. These matrices propagate an uncertainty δA_k affecting the system onto GEP (10): then, for a given uncertainty δA_k we must define matrices $\mathcal{D}^{\ell}_{i,k}$, $\mathcal{E}^{\ell}_{i,k}$ depending on whether value $(\theta^{\ell}_1 - \tau_i)$ belongs to Ω_1 or Ω_2 for $\ell = 1, \dots, M$, $i = 1, \dots, m$:

- if $(\theta^{\ell}_1 - \tau_i) \in \Omega_1$, then

$$\mathcal{D}^{\ell}_{i,k} = \begin{bmatrix} 0 & \dots & \overset{M+2+\ell}{\overset{\uparrow}{1}} & \dots & 0 \end{bmatrix}^{\top} \otimes D_{i,k}(\theta^{\ell}_1),$$

$$\mathcal{E}^{\ell}_{i,k} = \Big[\underbrace{0 \otimes I_n \ \dots \ 0 \otimes I_n}_{n \times (M+1) \text{ columns}} \ E_{i,k}(\theta^{\ell}_1) T_0\left(g_1(\theta^{\ell}_1 - \tau_i)\right) \ \dots \ E_{i,k}(\theta^{\ell}_1) T_M\left(g_1(\theta^{\ell}_1 - \tau_i)\right)\Big];$$

- if $(\theta^{\ell}_1 - \tau_i) \in \Omega_2$, then

$$\mathcal{D}^{\ell}_{i,k} = \begin{bmatrix} 0 & \dots & \overset{M+2+\ell}{\overset{\uparrow}{1}} & \dots & 0 \end{bmatrix}^{\top} \otimes D_{i,k}(\theta^{\ell}_1),$$

$$\mathcal{E}^{\ell}_{i,k} = \Big[E_{i,k}(\theta^{\ell}_1) T_0\left(g_2(\theta^{\ell}_1 - \tau_i)\right) \ \dots \ E_{i,k}(\theta^{\ell}_1) T_M\left(g_2(\theta^{\ell}_1 - \tau_i)\right) \underbrace{0 \otimes I_n \ \dots \ 0 \otimes I_n}_{n \times (M+1) \text{ columns}}\Big].$$

Observe that for more general cases ($NT \le \tau_m < (N+1)T$, $N \ge 1$) the definition of $\mathcal{D}^{\ell}_{i,k}$ does not change, while the definition of $\mathcal{E}^{\ell}_{i,k}$ simply depends on the subinterval Ω_j to which the value $(\theta^{\ell}_1 - \tau_i)$ belongs.

Algorithm 1 Computation of the Floquet *pseudospectral radius*.

Require: Problem data: $A_i, D_i, E_i, \tau_i, \varepsilon$, tolerance η, scaling factor $h > 1, n_{\text{start}} = 3$.

For $\ell = 1, \dots, M$, for $i = 1, \dots, m$, and for $k = 1, \dots, K$ define matrices $\mathcal{D}_{i,k}^{\ell}$ and $\mathcal{E}_{i,k}^{\ell}$.

Solve GEP (10) and for $i = 1, \dots, n_{\text{start}}$ store the i-th largest eigenvalue $\mu(i)$ and the corresponding eigenvectors $x(i)$ and $y(i)$ s.t. $x(i)^* \mathcal{A} y(i) > 0$.

for $i = 1 : n_{\text{start}}$ **do**

  Set $\mu_{i,1} = \mu(i)$, $x_{i,1} = x(i)$, $y_{i,1} = y(i)$.

  Initialize perturbations $\delta A_1^*, \dots, \delta A_K^*$ using equations (27).

  For $k = 1, \dots, K$ define $\delta \mathcal{B}^{(k)}$ and the perturbed GEP (22).

  Solve the GEP and set $\mu_{i,2}$ equal to the largest eigenvalue and $x_{i,2}$, $y_{i,2}$ equal to its left and right eigenvectors.

  Set $\zeta = +\infty$, $n = 2$, $r_n = 1$, $\delta A_{k,n} = \delta A_k^*$.

  while $\zeta > \eta$ **do**

    Compute the derivatives $\delta \dot{A}_{k,n}$ for $k = 1, \dots, K$ using formulas (29) and (30).

    Compute

$$\delta \widehat{A}_{k,n+1} = \delta A_{k,n} + r_n \delta \dot{A}_{k,n}, \quad k = 1, \dots, K.$$

    For $k = 1, \dots, K$, normalize if necessary

$$\delta A_{k,n+1} = \begin{cases} \delta \widehat{A}_{k,n+1}, & \text{if } \left\| \delta \widehat{A}_{k,n+1} \right\|_F \le \varepsilon, \\ \dfrac{\varepsilon \delta \widehat{A}_{k,n+1}}{\left\| \delta \widehat{A}_{k,n+1} \right\|_F}, & \text{otherwise.} \end{cases}$$

    For $k = 1, \dots, K$ define $\delta \mathcal{B}^{(k)}$ and the perturbed GEP (22).

    Solve the GEP and set $\hat{\mu}$ equal to the largest eigenvalue and $\hat{x}$, $\hat{y}$ equal to its left and right eigenvectors.

    Set $r = r_n$.

    while $|\hat{\mu}| \le |\mu_{i,n}|$ **do**

      Set $r = r/h$ and repeat steps from 11 to 14 with step r.

      Solve the GEP and set $\hat{\mu}$ equal to the largest eigenvalue and $\hat{x}$, $\hat{y}$ equal to its left and right eigenvectors.

    end while

    if $r < r_n$ **then**

      Set $\mu_{i,n+1} = \hat{\mu}, x_{n+1} = \hat{x}, y_{n+1} = \hat{y}, r_{n+1} = r$

    else

      Set $\tilde{r} := h r_n$ and repeat steps from 11 to 14 with step $\tilde{r}$.

      Solve the GEP and set $\tilde{\mu}$ equal to the largest eigenvalue and $\tilde{x}$, $\tilde{y}$ equal to its left and right eigenvectors.

      if $|\hat{\mu}| \le |\tilde{\mu}|$ **then**

        Set $\mu_{i,n+1} = \tilde{\mu}, x_{i,n+1} = \tilde{x}, y_{i,n+1} = \tilde{y}, r_{n+1} = \tilde{r}$

      else

        Set $\mu_{i,n+1} = \hat{\mu}, x_{i,n+1} = \hat{x}, y_{i,n+1} = \hat{y}, r_{n+1} = r_n$

      end if

    end if

    Set $\zeta = \dot{\mu}_{i,n+1}$ and $n \to n + 1$.

  end while

  Set $\mu_i = \mu_{i,n+1}$.

end for

return $\mu_\varepsilon = \mu_{i^*}$ s.t. $|\mu_{i^*}| = \max_{i=1,\dots,n_{\text{start}}} |\mu_i|$.